Geological Society of America
Reviews in Engineering Geology, Volume XV
2002

Landslides resulting from structural failure of volcanoes

Lee Siebert
Smithsonian Institution, Global Volcanism Program, NMNH MRC-119, Washington, D.C. 20560 USA

ABSTRACT

The relatively recent appreciation of the geological significance of large volcanic landslides has led to their identification at several hundred volcanoes. The morphological and textural similarities of volcanic debris-avalanche deposits to those of nonvolcanic landslides facilitated their recognition, but there are also significant differences between the two landslide varieties. Volcanic landslides are often larger (by two or more orders of magnitude) and are substantially more mobile than nonvolcanic landslides. This reflects factors including the mobility-enhancing influence of volcanic fluids, gases, and explosions, and material properties effects such as the greater component of fragmental materials that form volcanoes. Failure planes of volcanic landslides are typically substantially deeper than those of nonvolcanic landslides, often reaching 1–2 km depth.

Large-scale edifice failure occurs at volcanoes ranging from <10 to >10 000 km^3 in size. Typically <10% of an edifice fails, but multiple failures can occur as renewed eruptions reconstruct the edifice. The ensuing volcanic debris avalanches travel far beyond the flanks of a volcano (<10 to >100 km) at velocities that may approach 100 m/s, covering areas of <10 to >1000 km^2. Morphology, textures, and emplacement mechanisms vary with water content; avalanches can be relatively dry, or sufficiently wet to transform into lahars. In addition to hazards from the avalanches, landslides from coastal volcanoes have produced tsunamis; volcanic landslides can trigger, or be accompanied by, eruptions that produce hazards from lateral blasts, Plinian explosions, pyroclastic flows, and lahars.

INTRODUCTION

Landslides at volcanoes share many of the attributes of landslides in nonvolcanic terrain. The similarity of morphology and texture of many volcaniclastic deposits extending beyond the flanks of volcanoes with those of landslide deposits in other mountainous terrain led to the relatively recent recognition that these major mass movements are also common at volcanoes. Volcanic landslides, however, tend be dramatically larger and more mobile than their nonvolcanic counterparts. Although volcanic landslides can occur in the absence of eruptions, active volcanic processes provide additional triggering agents and can influence avalanche mobility. Millions of people today live on top of large volcanic debris-avalanche deposits, attracted by volcanically enriched soils and topographically subdued surfaces of volcaniclastic deposits suitable for both agriculture and urban centers. The potential hazards of these massive landslides are compounded by difficulties of recognizing precursors of variable nature and duration.

The terminology of rapid mass movements in both volcanic and nonvolcanic terrains is variable; an abbreviated list includes rockslide avalanche, rockfall avalanche, rock avalanche, debris avalanche, debris flow, and sturzstrom. Although volcanic mass movements begin with sliding, flow soon dominates, reflected in the two most commonly used terms in a volcanological context, i.e., debris avalanche and debris flow. The term debris flow is less desirable because of overlap with the more restricted volcanological use of debris flow in lahar studies to refer to water-saturated mass movements transitional between hyperconcentrated flows and debris avalanches (Pierson and Costa, 1987; Smith and Lowe, 1991). The water content of volcanic debris avalanches varies from largely dry to, at the other extreme, sufficient water content

Siebert, L., Landslides resulting from structural failure of volcanoes, *in* Evans, S.G., and DeGraff, J.V., eds., Catastrophic landslides: Effects, occurrence, and mechanisms: Boulder, Colorado, Geological Society of America Reviews in Engineering Geology, v. XV, p. 209–235.

to cause transformation into lahars (debris flows sensu stricto). Massive volcanic slope movements range from slow, long-term slumping to high-velocity debris avalanches. This chapter focuses on large (10^8–10^{12} m^3) rapid volcanic slope failures, factors contributing to their initiation and transport, and characteristics of resulting deposits and associated eruptive phenomena.

FREQUENCY OF OCCURRENCE

For many years catastrophic structural failure of volcanoes was thought to be largely restricted to vertical collapse associated with magma chamber evacuation and ensuing caldera formation. However, large-scale slope failure producing lateral displacements has been found to be a common form of volcano instability (Voight et al., 1981; Ui, 1983; Siebert, 1984; Ui et al., 1986b; Francis and Self, 1987; Siebert et al., 1987). Large landslide deposits have been recognized in a variety of tectonic settings at volcanic landforms ranging from lava dome complexes to massive shield volcanoes. Massive slope failure deposits and/or their source areas are now recognized at more than 350 Quaternary volcanoes, including more than 1 out of 6 of the world's Holocene volcanoes (listed in Simkin and Siebert, 1994). This is certainly a minimum figure; many volcanoes have yet to be investigated in sufficient detail to identify avalanche deposits. In a well-studied region such as Japan, debris avalanches have been documented at more than 40% of volcanoes (Ui and Fujiwara, 1993).

It was initially assumed that this form of massive structural failure could occur only once or twice in the life cycle of a volcano, but studies have revealed evidence for repetitive collapse at many volcanoes. Large-scale edifice collapse has occurred from ~6–12 times at Myoko volcano in Japan (Kawachi and Hayatsu, 1994), Mexico's Las Derrumbadas lava dome complex (Siebe et al., 1993), Mauna Loa on the island of Hawaii (Moore et al., 1994), Egmont in New Zealand (Palmer et al., 1991), Shiveluch volcano in Kamchatka (Voight et al., 1994), Augustine in Alaska (Begét and Kienle, 1992; Waitt and Begét, 1996), and Colima in Mexico (Komorowski et al., 1997). Although these frequencies are not typical, such repetitive failure is possible following rapid reconstruction of the edifice at volcanoes with high magma extrusion rates. Yoshimoto and Ui (1997) reported evidence for two independent sector failures oriented perpendicularly to each other during a single eruption at Komaga-take volcano in Japan.

FACTORS CONTRIBUTING TO STRUCTURAL FAILURE

The inherent instability of volcanoes is attributable to a large number of factors, acting individually or in concert. Although these destabilizing conditions (Fig. 1) often persist over long times, failure can occur suddenly, accompanying eruptions or in their absence. The high relief and steep slopes of many stratovolcanoes favor collapse; Francis and Wells (1988) noted a correlation between edifice height and collapse frequency of central Andes volcanoes. However, failure also occurs at much smaller lava dome complexes and at low-angle shield volcanoes, reflecting instability-enhancing volcanic processes not present in nonvolcanic mountainous terrain. Structural factors such as steep dip slopes of interbedded competent lavas and unconsolidated pyroclastic materials, construction of asymmetrical edifices along inclined basement surfaces (Leonov, 1995; Vallance et al., 1995), and displacement promoted by intrusion of parallel dike swarms (Siebert, 1984) or at intersecting rift zones (Carracedo, 1996) all contribute to instability. At coastal volcanoes the debuttressing effect of marine erosion and changes in sea levels are destabilizing factors that produce preferential failure in a seaward direction (McGuire, 1996). Van Wyk de Vries and Borgia (1996) noted the effect of the type and rheology of volcanic substrates on volcano deformation.

Elevated fluid pressures that can lower yield strengths of rock masses result from several processes. Hydrothermal alteration can convert large segments of the upper edifice to clay minerals (López and Williams, 1993; Frank, 1995). Day (1996) argued that the ensuing instability results not so much from reduction of the coefficient of friction of altered rock masses, but from increased permeability that elevates pore-fluid pressures. Saturation of portions of the edifice by hydrothermal waters accompanying magmatic intrusions (Voight et al., 1983) or dike emplacement (Ellsworth and Voight, 1995) can elevate fluid pressures, weakening the edifice. Modeling by Reid (1994) suggests that fluid pressures can remain above hydrostatic levels for 10^3–10^4 yr as a result of thermal pressurization produced by magma intrusion at depth.

Most volcanoes are susceptible to massive gravitational slope failures that can occur in the absence of dynamic triggering agents such as magmatic intrusions and explosive eruptions; this is disturbing from a hazards perspective. However, one or more dynamic mechanisms often precipitate the collapse of structurally weakened edifices. Earthquakes are inferred to play a significant role in the initiation of large volcanic landslides, as is the case in nonvolcanic terrain (where heavy rainfall can be a more frequent triggering

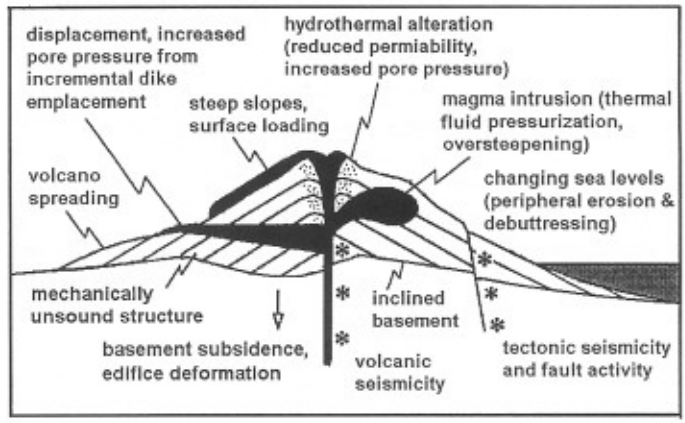

Figure 1. Factors contributing to structural instability of volcanic edifices (modified from McGuire, 1996).

agent; Eisbacher and Clague, 1984). Magmatic intrusions at Bezymianny volcano in Kamchatka in 1956 (Gorshkov, 1959) and Mount St. Helens in 1980 (Voight et al., 1981, 1983) produced major deformation, and earthquakes precipitated edifice failure.

Phreatic eruptions are often invoked as a triggering agent for slope failures, including cases where no explosive products have been identified (Kawachi and Hayatsu, 1994). Even where explosive activity is documented, however, the relative timing of explosions and collapse is often poorly known. The 1772 Papandayan collapse in Java (Glicken et al., 1987) and the 1888 Bandai-san collapse in Japan (Sekiya and Kikuchi, 1889) were accompanied by and may have been triggered by phreatic explosions, although some uncertainty surrounds the precise timing of the collapse at Bandai. Deposits of the 1964 debris avalanche at Shiveluch volcano in Kamchatka have been considered to have been produced by magmatic explosive eruptions, but stratigraphic studies have shown that the avalanche preceded all explosive activity (Belousov, 1995). Although explosive eruptions often accompany collapse, and may sometimes precipitate it, the role of volcanic explosions in initiating volcano collapse may be overstated. In contrast, explosions may be triggered by failure of the edifice, which suddenly removes overburden above volcanic conduits, rapidly depressurizing the magmatic or hydrothermal systems within or beneath the volcano.

SOURCE AREAS

Source areas of volcanic landslides form massive reentrants into the edifice that open in the downslope direction. Many nonvolcanic landslides originate along bedding planes, whereas volcanic landslides are deeper seated (Fig. 2) and not as influenced by stratigraphic dip slopes. Often 1 km or more of the volcano's summit can be removed, forming steep headwalls that rise above low-angle crater floors. This low-angle basal failure plane of volcanic landslides is in contrast to the 25°–50° slope (e.g., Cruden, 1976) common at many nonvolcanic landslides. This morphology is accentuated when collapse is accompanied by major explosions.

The trajectories of least principle stress in quasiconical volcanic constructs are roughly circular; failure perpendicular to this direction produces horseshoe-shaped failure scarps that commonly incorporate the former summit (Fig. 3). Volcanoes vary widely in morphology, however, and failure scarps can in plan view include <15°–120° of the edifice (Francis and Wells, 1988; de Silva et al., 1993; Ui and Fujiwara, 1993). The width of volcanic landslide scarps ranges from <1 to >10 km. The mean width (n = 149) perpendicular to the breached direction is 2.5 km (Siebert, 1996), a size comparable to small collapse calderas. Calderas formed by avalanches often differ morphologically from erosional calderas, which narrow significantly in the breached direction (Siebert, 1984).

Some volcanoes, such as Bandai-san in Japan, retain remnants of failure scarps of several generations of collapse; more often scarps are largely or completely concealed by postcollapse eruptions. Reconstruction need not be a lengthy process. In the 40 yr since its 1956 collapse, dome growth at Bezymianny volcano has risen above the crater walls. Small-volume volcanoes with high magma extrusion rates such as Augustine volcano are capable of restoring the edifice to pre-failure dimensions in less than a century (Siebert et al., 1989; Begét and Kienle, 1992).

BEHAVIOR AND MOBILITY

Initial movement of volcanic landslides involves block sliding, and at some volcanoes such as Socompa in Chile, coherent kilometer-scale slumped blocks are present in proximal areas (Francis et al., 1985; Wadge et al., 1995). In most cases disaggregation rapidly transforms movement into fragmental flow, which on steep slopes rapidly attains high velocities that sustain rapid movement over low-angle terrain long distances beyond the volcano. The mobility of both nonvolcanic (Scheidegger, 1973; Hsü, 1975) and volcanic (Ui, 1983; Voight et al., 1983, 1985; Siebert et al., 1987; Hayashi and Self, 1992; Adushkin et al., 1995) avalanches is affected by the available vertical drop and by volume of the failure mass. Although the mobility of both types of avalanches is influenced by volume, data on a large number of volcanic avalanches show a pronounced increased mobility relative to nonvolcanic avalanches (Fig. 4). This is attributed to the availability of hydrothermal and magmatic fluids at volcanoes and to the greater percentage of fragmental material in volcanic source areas, facilitating fluid-particle interaction (Voight et al., 1985).

Although coeval explosive eruptions increase mobility (Glicken, 1986, 1996; Sousa and Voight, 1991; Clement et al., 1993), volcanic avalanches that occur in the absence of eruptions or active hydrothermal systems also display enhanced mobility over nonvolcanic avalanches, suggesting that differences in material properties of their respective source regions are important factors. The rapid onset of mobile flow during volcanic landslides is facilitated by the presence of fragmental pyroclastic and hydrothermally altered materials and the prefailure fracturing of more coherent materials by explosions, volcanic seismicity, and/or magmatic intrusions. The generation of large volumes of hydrous clay minerals through extensive hydrothermal alteration of areas adjacent to volcanic vent systems can provide fluids that enhance mobility (López and Williams, 1993; Carrasco-Núñez et al., 1993; Frank, 1995; Scott et al., 1995).

Estimated maximum velocities of volcanic debris avalanches of ~50–150 m/s have been back-calculated using kinematic analysis of avalanche deposits (Ui et al., 1986b; Eppler et al., 1987; Siebert et al., 1989; Sousa and Voight, 1991; Stoopes and Sheridan, 1992). The use of constant rheology models, however, results in overestimation of velocity and underestimation of emplacement time (Sousa and Voight, 1991, 1995). Empirical energy-line velocity calculations for the Mount St. Helens avalanche exceed those observed by a factor of about two (Ui et al., 1986b). At Mount St. Helens, the only volcano where direct avalanche velocities were obtained, the avalanche had a minimum initial velocity of ~70–80 m/s and an average velocity of ~35 m/s (Voight et al., 1981, 1983). Evidence for higher velocities at the

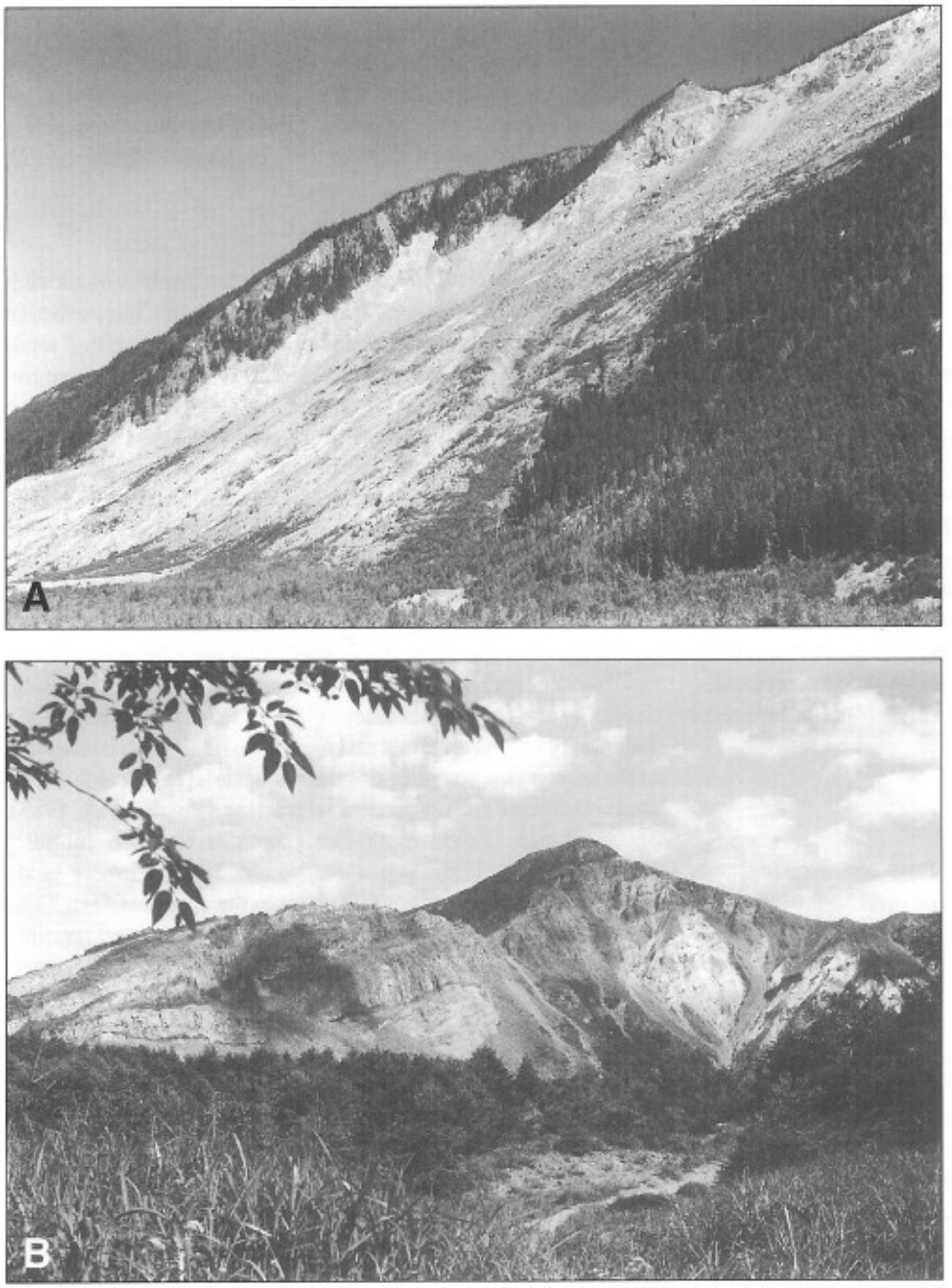

Figure 2. Contrasting morphology of nonvolcanic and volcanic landslide scarps. A: 1965 nonvolcanic landslide scarp at Hope, British Columbia (Mathews and McTaggart, 1969), is shallow with steeply sloping basal failure plane. B: Eastern half of 1888 landslide scarp at Bandai volcano, Japan (Sekiya and Kikuchi, 1889), where as much as 700 m of material was removed, leaving steep headwall rising above relatively flat basal failure plane in foreground. Note thick lava flow sequence in headwall overlying pyroclastic base.

base of the volcano may have been obscured by the rapidly expanding blast cloud (Sousa and Voight, 1991).

Volcanic debris avalanches behave rheologically as rapid inertial granular flows in which frictional effects are minimized by high basal shear rates (Voight et al., 1983; Pierson and Costa, 1987). Momentum is transferred by grain to grain dispersive forces, but above the basal shear surface, high yield strengths exceed shear stress, permitting Bingham-model rigid plug flow of discrete coherent masses for long distances. Yield strength and viscosity decrease dramatically with distance, contributing to high runout distances (Sousa and Voight, 1991). Flow is dominantly laminar; paleomagnetic measurements by Mimura et al. (1982) indicate that large clasts rotated in a horizontal but not vertical plane. Movement is not necessarily entirely passive, however, as evidenced by bedded tephra layers in the debris-avalanche deposit from Raung volcano in Indonesia that often dip more steeply than plausible for primary dips (Siebert et al., 1996). Reynolds numbers of 20–40 for the Mount St. Helens avalanche are substantially lower than common for the transition from laminar to turbulent flow (Voight et al., 1983); however, turbulent flow may be locally important, particularly in explosively motivated avalanches (Glicken, 1986, 1996; Sousa and Voight, 1995).

Figure 3. Holocene landslide removed summit of Pacaya volcano, Guatemala (Vallance et al., 1995); postcollapse volcanism has constructed MacKenney cone to elevation above landslide scarp. South wall of failure scarp is seen at right; north wall forms small peak barely visible at middle left skyline. Historical lava flows from MacKenney cone cover low-angle failure plane; debris-avalanche hummock forms foreground.

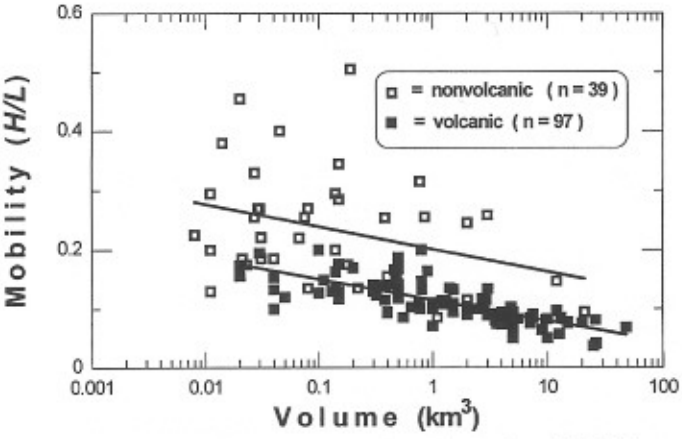

Figure 4. Semilogarithmic comparison of mobility (ratio of fall height to travel distance, *H/L*) and volume of nonvolcanic (data from Voight et al., 1985) and volcanic debris avalanches.

Undulating avalanche trimlines to 200 m above a valley floor at Mount St. Helens (Fisher et al., 1987) provide evidence for transient wave-like transport that left thin veneers well above valley-floor deposits (Fig. 5).

Hydrothermal and magmatic fluids entrained within avalanches contribute to their mobility, but fluidization by gas is incomplete. The Inman (1952) sorting coefficients for debris from the Mount St. Helens (Voight et al., 1983; Glicken, 1986, 1996) and other volcanic avalanches (Fig. 6) are higher than the upper limit of ~1 that is required to sustain fluidization (Wilson, 1980). Temperatures of volcanic landslides are generally considered to be low (<98 °C at Mount St. Helens; Voight et al., 1981), even when accompanied by magmatic eruptions. Clement et al. (1993) calculated temperatures averaging 360 °C from paleomagnetic evidence at the Nevado de Colima avalanche in Mexico, although these temperatures may not have characterized the avalanche as a whole. Although carbonized wood is found in avalanche deposits at Colima, implying at least localized temperatures in excess of ~400 °C, this in part may result from incorporation of wood charred by associated pyroclastic flows or surges or noneruptive processes (Komorowski et al., 1997). Despite the incorporation of large amounts of magmatic materials in the Mount St. Helens avalanche, blocks of glacial ice littered the avalanche surface and were exposed in excavations several years later. Even lower temperatures are likely at many other avalanches less affected by magmatic processes, and the variable proportions of interstitial water and air in volcanic avalanches also influence mobility and flow behavior. Many avalanches are largely dry, but others often contain or incorporate variable amounts of water, at one extreme in sufficient quantity to transform into lahars that travel greater distances.

A wide variety of models, only mentioned here, have been proposed to account for the increased mobility of debris avalanches over predicted models for sliding or grain flow (Hsü, 1975). Models commonly invoke reduced friction resulting from factors such as compressed air layers (Shreve, 1968), intergranular dust (Hsü, 1975), melting along the slide plane (Erismann, 1979), or fluidization by air (Kent, 1966), by vaporized water (Habib, 1975), or by acoustical vibration (Melosh, 1979). Davies (1982) invoked a mechanical fluidization through grain to grain dispersive forces. The thin basal shear zone found at many dry nonvolcanic landslides (Yarnold and Lombard, 1989) is predicted by mathematical modeling (Campbell, 1989). The grain-dispersive models, in which the bulk of an avalanche flows as a relatively inactive mass of high yield strength above a thin layer of highly

Figure 5. Diagonal contact near top of photo marks trimline dividing dark colored lateral–blast tree blowdown above lighter colored valley walls scoured from 30 to 200 m height by undulating transport of Mount St. Helens debris avalanche. Valley-floor avalanche deposit here is overlain by flat-lying secondary pyroclastic-flow deposits originating from lateral blast.

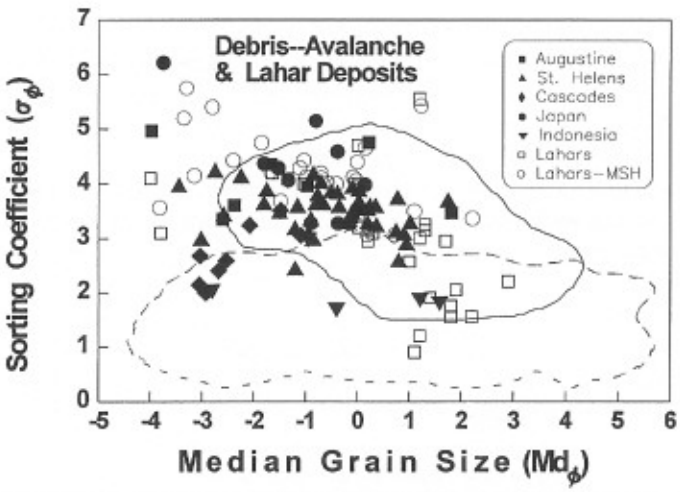

Figure 6. Size parameters of debris-avalanche deposits (black symbols) compared with those of lahars (white symbols), including data from Augustine (Siebert et al., 1989), Mount St. Helens (Glicken, 1986, 1996), Cascade Range and Indonesia (Siebert et al., 1995), Japan (Murai, 1961), lahar data (Walker, 1971), and Mount St. Helens (MSH) southwest flank lahars (Major and Voight, 1986). Data point locations may vary slightly because of differing sampling and analytical procedures. Solid and dashed lines outline, respectively, pyroclastic flow and Plinian air-fall fields of Walker (1971).

agitated particles, appear to account for the great mobility and many of the physical properties of landslides. Later modeling by Campbell et al. (1995), however, suggests that shearing, decreasing distally, can occur through much of the vertical extent of the avalanche. This would be expected to produce the pronounced change in aspect ratio from the initial failure slide blocks to the thinner distal avalanche.

MORPHOLOGICAL AND TEXTURAL CHARACTERISTICS OF DEBRIS-AVALANCHE DEPOSITS

Texturally and morphologically, deposits from volcanic debris avalanches are similar to those of many nonvolcanic rock avalanches, although their scale differs. The largest Quaternary subaerial volcanic deposits exceed 10 km^3 in volume and cover areas of hundreds of square kilometers to >1000 km^2 (Table 1); those of oceanic shield volcanoes can have volumes two orders of magnitude larger.

The surface morphology of debris-avalanche deposits is usually characterized by a hummocky terrain with numerous small hills and closed depressions. Surface drainage is often irregular or discontinuous, and small lakes or ponds may form in depressions. Distally, areas of flat surfaces may increase, and in some avalanche deposits hummocky morphology is subdued or largely absent (Francis and Wells, 1988; Siebe et al., 1993). Longitudinal ridges may also be prominent, as seen in many Martian examples (Lucchitta, 1979). In some instances, segments of a volcano can slide downslope as largely intact masses without transforming into debris avalanches. Large tilted and rotated blocks on a scale of several kilometers, termed toreva blocks, slid almost 7 km from their source at Socompa volcano in a nearly coherent manner without disaggregating like the bulk of the avalanche (Francis et al., 1985; Wadge et al., 1995).

Hummock size for subaerial deposits ranges from ~1 m to several hundred meters in height and >1 km in length, the long axes often being oriented parallel or perpendicular to transport direction. Portions of some avalanche deposits contain hundreds to thousands of closely spaced hummocks (Fig. 7); elsewhere hummocks are fewer and more widely spaced. Hummock height

TABLE 1. LARGE (≥5 km^3) QUATERNARY DEBRIS-AVALANCHE DEPOSITS

Volcano	Volume* (km^3)	Area (km^2)	Distance† (km)	References§
Shasta (Cascades)	46	675	49	Crandell (1989)
Nevado de Colima (Mexico)	22–33	2200	120	Stoopes and Sheridan (1992), Komorowski et al. (1997)
Socompa# (Chile)	26	606	37	Wadge and Francis (1995), Francis et al. (1985)
Raung (Indonesia)	25	1045?	79	Siebert et al. (1996), Neumann van Padang (1939)
Pico de Orizaba** (Mexico)	20?	350?	70?	Carrasco-Núñez et al. (1997)
Galunggung (Indonesia)	16	170	23	Bronto (1989)
Meru (Tanzania)	10–20	1400	50	Cattermole (1982)
Antuco (Chile)	15	200?	>30	Moreno (1991)
Fuego (Guatemala)	15	420	50	Siebert et al. (1994), Vallance et al. (1995)
Canlaon (Phillipines)	13	400	33	Geronimo-Cantane (1997)
Wrangell (Alaska)	>12.6	840	70	Yehle and Nichols (1980)
Shiveluch (Kamchatka)	>10	350	40	Belousova (1994)
Planchon–Peteroa†† (Chile)	>10	370	78	Naranjo et al. (1997), MacPhail (1973)
Yatsugatake (Japan)	>9	--	28	Mason and Foster (1956), Mimura et al. (1982)
Popocatépetl (Mexico) §§	>9	300	60	Siebe et al. (1995), Robin and Boudal (1987)
Colima (Mexico)	6–12	1200	48	Stoopes and Sheridan (1992), Komorowski et al. (1997)
Egmont (New Zealand)	>7.5	>250	>26	Palmer et al. (1991)
Avachinsky## (Kamchatka)	7–8	300	>30	Melekestsev et al. (1992)
Mawenzi (Tanzania)	7.1	1875	60	Downie and Wilkinson (1972)
Drum (Alaska)	>7	>200	85?	Richter et al. (1979)
Egmont (New Zealand)	5.8	>500	>39	Palmer et al. (1991)
Toluca (Mexico)	>5	500	55	Macias et al. (1997)
Acatenango*** (Guatemala)	5	210	41	Siebert et al. (1994), Vallance et al. (1995)
Kurohime (Japan)	5?	--	>25	Kawachi and Hayatsu (1994)
Iizuna (Japan)	5?	--	17	Kawachi and Hayatsu (1994)

*Submarine deposits from oceanic shield volcanoes are not included in this table. Data are unavailable for other large subaerial deposits. Volume data may include coeval lahar deposits (excluding postavalanche lahars extending beyond the avalanche deposit) and entrained accidental material through bulking during emplacement. The relative position of avalanche deposits in this table is only approximate; volumes are difficult to precisely determine primarily because accurate data on deposit thickness are often unavailable.

†Straight-line distance measured from source headwall (or volcano summit, when avalanche scarp is covered) to distal end of deposit.

§First reference for each volcano is source of volume data.

#Debris-avalanche deposit volume at Socompa is 25.7 km^3; an additional 44.5 km^3 of material remained within the source area in the form of rotated toreva and other slumped blocks (Wadge et al., 1995).

**Lahars extend beyond the ~70 km estimated extent of the Jamapa avalanche deposit inferred to originate from Pico de Orizaba (Citlaltepetl) to near the coast, 105 km from the volcano. More than one deposit may exist in the Jamapa drainage (Carrasco-Núñez, 1997, personal commun.).

††Straight-line travel distance is about 78 km; published reports of length of travel path along river valleys range from 87 to 100 km.

§§Average individual volume of 3 overlapping debris-avalanche deposits at Popocatépetl with a total volume of 27 km^3 (Siebe et al., 1995).

##A second avalanche of comparable volume underlies this deposit (Melekestsev et al., 1992).

***Chemistry of rocks from this debris-avalanche deposit from the Fuego–Acatenango complex shows affinities to Acatenango rather than Fuego rocks (Basset, 1996).

and density often decrease away from the volcano (Ui, 1983; Siebert, 1984; Glicken, 1986, 1996; Crandell, 1989), reflecting progressive disaggregation of debris-avalanche blocks. Hummocks may form by extension when lateral spreading of a debris avalanche produces horst and graben structures (Voight et al., 1981, 1983), or may represent the original surface topography of debris-avalanche blocks rafted in finer grained material that subsequently drained away (Glicken, 1986, 1996; Crandell, 1989). Radially oriented hummocks may form by deceleration in response to basal or lateral shear as coherent blocks that resist basal shear are slowed and sculpted by adjacent faster moving material into elongated hummocks parallel to flow direction (Glicken, 1986, 1991). Some transverse hummocks originate from compression resulting from deceleration when an avalanche encounters topographic irregularities (Eppler et al., 1987) or enters a body of water (Siebert et al., 1995).

Unlike many mudflow deposits, avalanche deposits often have sharply defined margins with marginal levees and a steep terminus. Levees can form on broad unconfined slopes as well as along confining valley walls and result from deposition of plug-flow material at a lower velocity flow margin where yield strength exceeds shear strength (Glicken, 1986, 1996). Levees may be subdued or absent at avalanches with higher water content. Steep-sided distal margins of dry avalanche deposits imply rapid cessation of movement. At Jocotitlán volcano inertial movement caused large airborne clasts to fall into lake sediments several hundred meters beyond the avalanche terminus (Siebe et al., 1992). Substrate deformation, more pronounced distally, has been observed at landslide deposits of nonvolcanic and volcanic origin (Yarnold and Lombard, 1989; Siebe et al., 1992). Scouring of preavalanche substrate may produce significant bulking through incorporation of valley-floor soil or sediments. At Mount

Figure 7. Closely spaced hummocks to 30 m high are prominent at West Island debris-avalanche deposit, Augustine volcano, Alaska. Flat areas are underlain by lateral-blast deposit order of magnitude smaller than at Mount St. Helens.

St. Helens, distal parts of the avalanche deposit included jumbled trees and highway pavement fragments (Glicken, 1986, 1996).

Large-scale textural features of volcanic debris-avalanche deposits (Table 2) have been described at many volcanoes, although thorough three-dimensional characterization of deposits is inhibited by the lack of vertical dissection of Quaternary deposits. Described deposits are typically poorly sorted and poorly graded, unstratified diamictons that contain large to very large dominantly angular to subangular clasts in a finer grained matrix. Clasts are often highly fractured, and debris-avalanche blocks that include massive lava flow or dome segments may be so pervasively shattered that, although their stratigraphy is locally preserved, their original texture is unrecognizable. Color mottling produced by the juxtaposition of distinct material of differing lithologies on a scale from centimeters to many meters is a prominent characteristic of the block facies of avalanche deposits. Fractured clasts of one lithology surrounded by crushed fragments of the same lithology appear in sharp to diffuse juxtaposition along horizontal to irregular contacts with clasts and matrix of another lithology.

Radial fracture patterns or an irregular fracture network termed "jigsaw cracks" (Shreve, 1968; Ui, 1983), in which fragments of adjacent clasts can visually be refitted across fractures millimeters to decimeters wide, are common. This fracture style differs from cooling joints in lava flows, chilled dike margins, or prismatic fractures of juvenile fragments in pyroclastic-flow deposits (Ui, 1987). Campbell et al. (1995) concluded from mathematical modeling that jigsaw-crack formation is a late-stage process, although Ui et al. (1986a) noted that the number of jigsaw cracks at an avalanche deposit in New Zealand did not vary with distance, suggesting formation during compression early in the sliding stage of movement. Elsewhere, shattering may be more pervasive, preserving fewer jigsaw fractures.

Scanning electron microscope images show that extensive fracturing extends to a microscopic level. Both block facies and mixed facies show fracturing of crystals, glass, and lithic fragments, along with the development of hackly surfaces on projecting segments of grains. Both features are apparently unique to debris-avalanche deposits (Glicken, 1991; Komorowski et al., 1991). The former is inferred to result from propagation of compression-rarefaction stress waves prior to disaggregation during early sliding stage movement, and the latter is inferred to result from high-pressure grain to grain contact early in the transport process.

Basal zones as thick as 5 m, wherein penetrative shear fragmented clasts and smeared out the fabric of avalanche blocks and produced a crude layering, are a common feature of nonvolcanic landslide deposits (Yarnold and Lombard, 1989), but evidence of pervasive shear can rapidly decrease vertically. Thin clastic dikes, typically several meters or more in length formed by injection of

TABLE 2. MORPHOLOGICAL AND TEXTURAL CHARACTERISTICS OF DEBRIS-AVALANCHE AND RELATED FACIES

Facies	Description	Morphology	Geometry
Block facies	Debris-avalanche blocks consist of coherent massive to highly brecciated and fragmented segments of the former edifice, transported relatively intact. Sharp-to-diffuse, planar-to-irregular contacts between individual edifice segments from centimeters to hundreds of meters in size can produce a pronounced color mottling. Monolithologic clasts within individual edifice blocks are often surrounded by silty-sand matrix of crushed fragments of the same lithology. Clasts dominantly angular to subangular. Jigsaw cracks variable in frequency, shattered clasts often unrotated. Clastic dikes may be present. Delicate features such as tephra layers may be transported long distances.	Contains abundant hummocks and/or ridges ranging from a few meters to a few hundred meters or more in height. Orientation is variable, but often radial or transverse with respect to flow direction. Hummocks may be closely spaced and of variable slope angles. Interior and margins of hummocks may be offset by minor normal faulting not observable at surface. Hummocks form small islands when avalanche enters shallow seas or lakes.	Lobate or sheet-like when unconfined, shoestring when confined by valley walls. May have abrupt margins. Typically a few tens of meters to a hundred meters or more thick, covering a few tens to hundreds of square kilometers; submarine deposits from oceanic shield volcanoes often substantially larger.
Mixed facies	Homogenized, fine-grained, monochromatic matrix dominates, but may contain varying amounts and sizes of heterolithologic clasts and occasional transported debris-avalanche blocks. Often ungraded, unsorted, unstratified. Clasts dominantly angular to subrounded, matrix typically silty sand. May locally contain clast clusters, schlieren, wood fragments and secondary soil and rock fragments.	Planar to somewhat irregular surface. Low hummocks composed solely of mixed-facies material are rare. Individual block-facies hummocks or hummock clusters (themselves containing variable amounts of mixed-facies material) may be transported within mixed-facies material forming intra-hummock areas.	Sheet-like when unconfined, shoestring when confined. Typically not more than a few tens of meters thick, can cover many hundreds of square kilometers, often forming dominant component of distal part of avalanche.
Avalanche–derived lahars	Matrix-supported fabric, with rare brecciated clasts. Clasts dominantly subrounded to rounded, some subangular clasts. Matrix is thoroughly homogenized, has larger silt and clay content, and may be more compact; bulking of secondary clasts of soil, tephra, or other substrate material more common.	Mostly planar surface. Hummocks rare, although some individual block-facies hummocks or hummock clusters may be transported long distances.	Sheet-like when unconfined, covers much broader areas perpendicular to drainage channels than lahars not derived from avalanches.
Toreva blocks	Large coherent segments of the volcano that slid downslope without disaggregating; rotational sliding can produce a reverse dip towards the volcano. Toreva blocks are relatively uncommon in association with volcanic debris avalanches.	Typical planar surfaces may be disrupted by en echelon faults perpendicular to the downslope direction. Toreva block margins are often steep-sided in downslope direction; proximal side often filled in by postcollapse material.	Massive toreva blocks may reach several kilometers in size, and are typically longer perpendicular to failure direction. Thickness can reach several hundred meters.

Note: Modified from Glicken (1991) and Palmer et al. (1991).

avalanche matrix material into fractures during avalanche movement, are commonly observed (Glicken, 1986, 1996; Yarnold and Lombard, 1989). Although fracturing and smearing out of clasts occurs during emplacement, relatively passive movement of much of the avalanche allows large segments of the edifice to be transported relatively intact. Primary stratigraphic contacts including delicate features like tephra layers may be preserved during transport for long distances (Fig. 8). The more extensive shear proposed by Campbell et al. (1995) derives from modeling of motion of spheres of uniform dimension and thus may be more applicable to transport of mixed facies than block facies material (see following).

The basal contacts of volcanic debris avalanches show evidence both of erosive scour and relatively passive transport. Lengthy horizontal contacts can be observed above largely undeformed soft sediments in some areas; elsewhere striation of substrate material occurs, and scour can imbricate and incorporate substrate material, occasionally including large relatively undeformed and stratigraphically intact segments of sedimentary and fluvial material as wide as 100 m or more. Scour, abrasion, and large-scale capture of substrate material appears more likely in areas of higher slope angle and irregular topography, such as sharp breaks in slope.

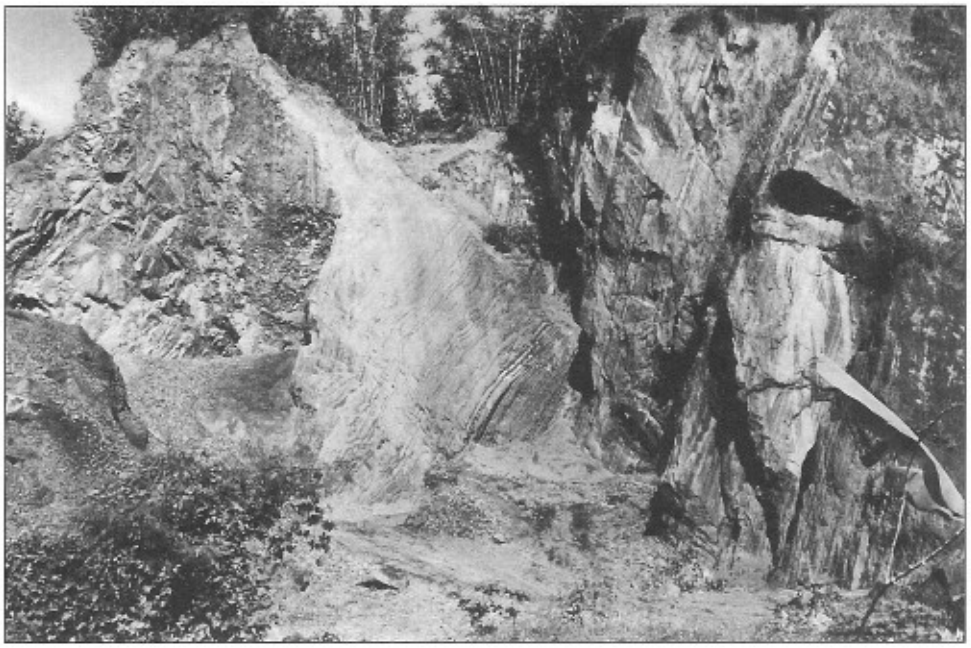

Figure 8. Lava-flow remnant on left overlying steeply dipping, slightly indurated transported tephra layers in block facies hummock ~30 km from Raung volcano, Java. Exposure is ~20 m high.

Debris-avalanche deposits are often divided into two texturally and sedimentologically different units, a block facies and a mixed facies (Glicken, 1991); the mixed facies has been referred to as matrix facies (Mimura et al., 1982; Ui, 1983, 1987; Crandell et al., 1984; Glicken, 1986). Although both facies contain coarse block sized as well as finer grained material, and may appear in the same outcrop, their appearance differs (Table 2). Block facies material, which dominates in most hummocks, consists of segments of the volcano transported relatively intact (Fig. 8). Each debris-avalanche block represents a single coherent edifice segment from centimeters to hundreds of meters in size and may contain many clasts of block-sized material as well as finer grained matrix. Block facies hummocks may consist of one large clast, multiple clasts of a single rock type, or multiple deformed and faulted clast groups of varying lithologies.

With progressive fragmentation, block facies material is transitional into mixed facies material that represents more homogenized parts of the avalanche and is texturally more similar to mudflow deposits. Although mixed facies material may contain small debris-avalanche blocks, it is dominated by finer grained, more monochromatic mixtures of material that are poorly graded and sorted and display little stratification. Although in proximal areas block facies material may dominate, in more distal areas block facies material may be a minor component within mixed facies and/or lahar facies material that forms broad intrahummock areas. Hummocks composed solely of mixed facies material are rare and usually less than a few meters high (Glicken, 1986, 1996), although many hummocks containing block facies material also contain variable amounts of more homogenized matrix.

At wetter avalanches in New Zealand, Palmer et al. (1991) distinguished a third facies consisting of avalanche material that had been transformed into lahars, was more thoroughly mixed, and contained few debris-avalanche blocks. In some cases, such as at Mount Rainier in the Cascade Range and Orizaba in Mexico, this facies may be volumetrically dominant. High water contents are thought to derive from pore space in clay-rich, hydrothermally altered rocks filled by melting of summit icecaps, causing early transformation of debris avalanches into lahars (Carrasco-Núñez et al., 1993; Scott et al., 1995).

Debris-avalanche particles vary from silt size to extremely coarse blocks, and deposits are usually poorly sorted and poorly graded. The inverse grading reported at some dry, nonvolcanic landslide deposits (Yarnold and Lombard, 1989) is not as prominent as at many lahar deposits (Scott, 1989), although Takarada (1991) noted normal grading of lithic fragments and reverse grading of wood fragments. Debris-avalanche clasts are largely angular to subangular, but rounding can increase distally due to abrasion and incorporation of rounded valley floor sediments (Ui et al., 1986a). Grain-size analysis of debris-avalanche deposits incorporating procedures to account for very coarse clasts at Mount St. Helens (Glicken, 1986, 1996) and Augustine (Siebert et al., 1989) show that avalanche deposits typically have a bimodal distribution and are more poorly sorted than pyroclastic-flow deposits. Avalanche size and sorting data (Fig. 6) show considerable overlap with data from lahar deposits, suggesting that larger scale textural characteristics are the more useful discriminators (Siebert et al., 1995). Determination of representative grain size and engineering properties data of volcanic debris-avalanche deposits is complicated by the wide range of clast sizes and the locally variable proportions of block facies and mixed facies material; to date these properties have been investigated in great detail only at the Mount St. Helens deposit (Voight et al., 1981, 1983; Glicken, 1986).

CASE STUDIES

Case studies of several volcanoes briefly illustrate the characteristics of large volcanic debris-avalanche deposits, the variety of volcanic landforms affected by slope failure, and the types of associated eruptive phenomena.

Mount St. Helens 1980

The 1980 collapse of Mount St. Helens was the first instance in which a major slope failure at a volcano was observed and documented as it occurred. It resulted in the most detailed study of a volcanic debris-avalanche deposit to date (Glicken, 1986, 1996), and was responsible for focusing the attention of volcanologists worldwide on what had been an underappreciated volcanic hazard. On May 18, following two months of earthquakes, deformation, and phreatic eruptions accompanying magma intrusion into the upper edifice, the summit collapsed. Collapse direction may have been influenced by deflection to the north of the rising magma body by the summit lava dome (Fig. 9), but the failure margin truncated existing structures on all sides. The initial rockslide rapidly disaggregated into a debris avalanche that reached an estimated velocity of >70 m/s by the time it reached the base of the volcano. The retrogressive landslide traveled in three major pulses as far as 26 km down the North Fork of the Toutle River (Fig. 10), accumulating to an average thickness of 45 m over an area of 60 km^2 (Voight et al., 1981, 1983; Glicken, 1986, 1996). The second and third landslide blocks (Fig. 9) were coincident with a lat-

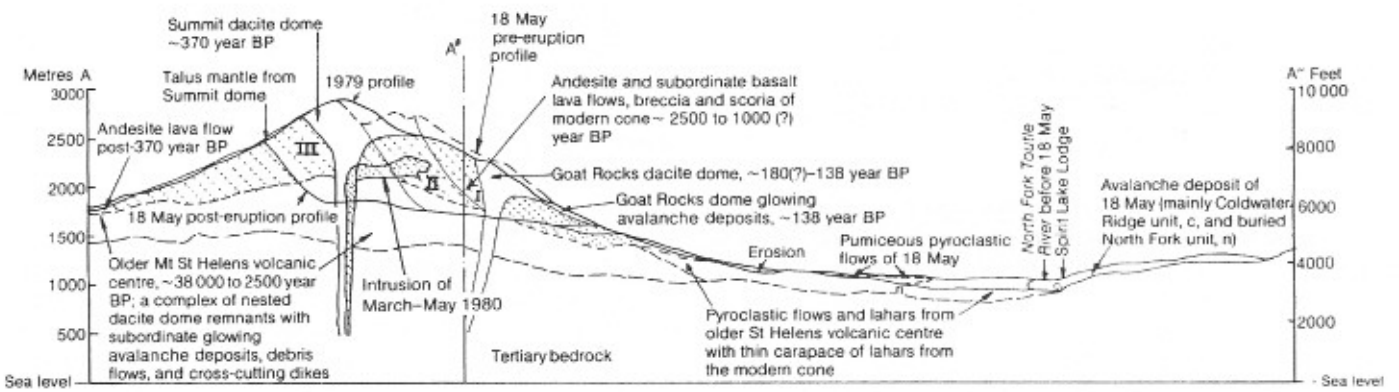

Figure 9. Cross-sectional view of 1980 collapse of Mount St. Helens showing prefailure and postfailure profiles and precollapse locations of slide blocks (Voight et al., 1983).

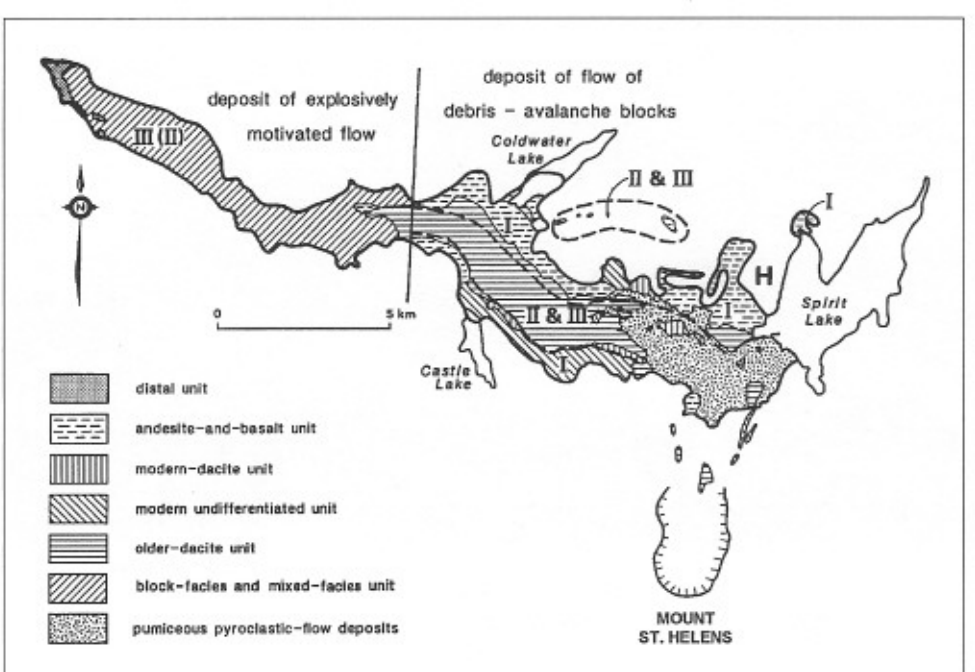

Figure 10. Map of 1980 Mount St. Helens debris-avalanche deposit (after Glicken, 1991). I, II, and III identify material from successive retrogressive slide blocks.

eral blast that enhanced avalanche mobility. Both yield strengths and viscosities are an order of magnitude higher for the initial slide block than for the later slide blocks (Sousa and Voight, 1995). Calculated shear strengths ranged from 0.02 to 0.2 bar (Voight et al., 1983); Glicken (1986, 1996) noted that shear increased where the avalanche passed over topographic irregularities.

The degree of fragmentation of the Mount St. Helens avalanche exceeds that of many other avalanches, in part resulting from disruption by blast explosions. The largest exposed clast is 15 m long and 6.2 m high (Glicken, 1986); larger clasts are found elsewhere in avalanches an order of magnitude smaller. Most fragmentation of avalanches is thought by Glicken (1986, 1996) to occur near the source; the size and sorting parameters of the Mount St. Helens deposit did not vary appreciably with distance. Size data range, however, decreased with distance as a result of disaggregation and partial mixing during transport. Glicken (1986) calculated a maximum water volume of 15% in the deposit, most of which was derived from groundwater within the prefailure edifice. Dewatering of the avalanche deposit produced a series of lahars with an average water content of 42% that traveled down the North Fork of the Toutle River beginning 5 h after the avalanche stopped (Fairchild, 1987).

The 1980 Mount St. Helens avalanche, like a very similar event at Bezymianny volcano in Kamchatka in 1956, occurred in association with major magmatic eruptions. Phreatic eruptions accompanied magmatic intrusions for 51 days prior to the May 18 slope failure, which led to a devastating lateral blast produced by rapid unroofing of the hydrothermal-magmatic system within the edifice by the landslide. Powerful Plinian explosions followed that deposited tephra across several states, accompanied by pumiceous pyroclastic flows that reached Spirit Lake. The eruption caused 57 fatalities, mostly due to the lateral blast, and produced severe economic disruption. Lahars swept as far as the Columbia River, destroying bridges and highways, and heavy ash fall caused great disruption over broad areas. The eruption ended following episodic lava dome growth that continued until 1986.

Bandai 1888

On July 15, 1888, following a week of increased seismicity, an eruption began with 15–20 rapid explosions on the north flank of Kobandai volcano, the northernmost of a group of overlapping andesitic stratovolcanoes forming Bandai volcano in north-central Honshu (Sekiya and Kikuchi, 1889). Eyewitnesses observed the last explosion to be projected almost horizontally northward, followed by growth of a 4-km-high vertical eruption column that produced ash fall to the Pacific coast. Failure of the north flank of Kobandai produced a 1.5 km^3 debris avalanche that buried several villages and traveled 11 km to the north, leaving a 1.5 × 2 km crater breached to the north (Fig. 11). Several large lakes subsequently formed along drainages blocked by the avalanche (Fig. 12).

In contrast to the Mount St. Helens event, no new magmatic material was found in either the avalanche or air-fall tephra deposits (Nakamura, 1978). A tephra deposit possibly originating from a lateral blast was found below the southeast rim of the source crater (Glicken and Nakamura, 1988), but no such deposits were found on or beyond the avalanche deposit to the north. Most of the 461 fatalities were caused by the north side debris avalanche, which covered 34 km^2, although some resulted from the associated lateral blast or pyroclastic surge that downed trees and houses on the southeast side. Three months after the avalanche, the breakout of Akimoto Lake, formed by the avalanche, produced downstream flooding. Collapse occurred at the juxtaposition of

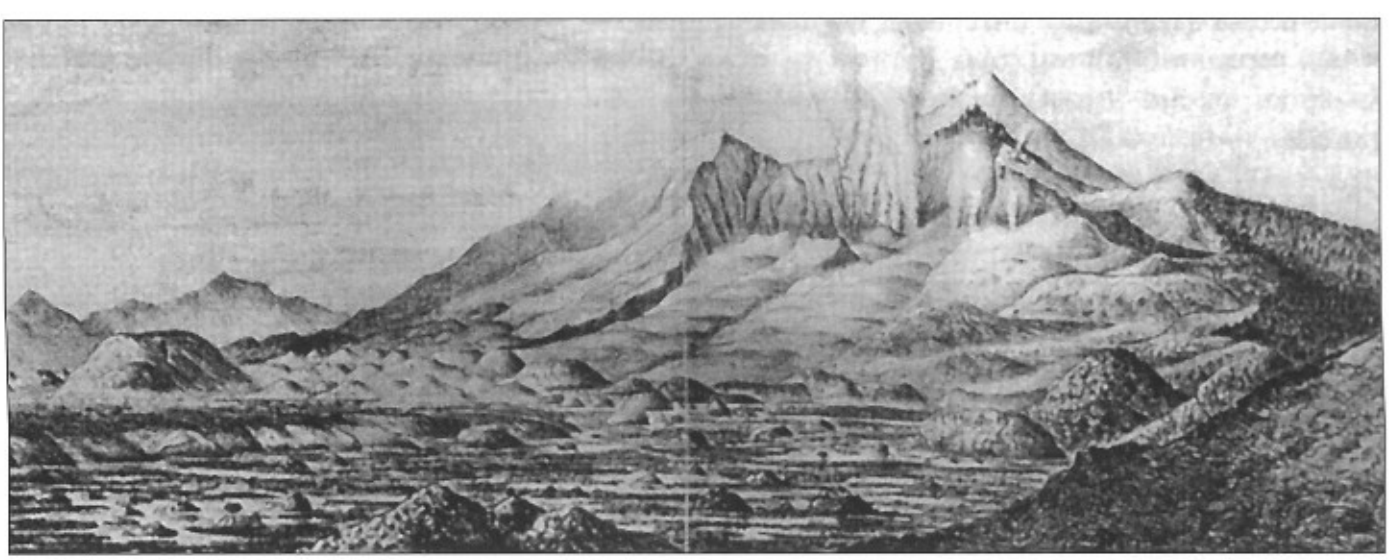

Figure 11. Sketch of 1888 Bandai debris-avalanche deposit from north about three weeks after eruption (Sekiya and Kikuchi, 1889) showing steaming fissure within avalanche source area. Foreground hummocks were later covered by rising waters of Lake Hibara. Obandai peak forms summit high point, dark jagged peak immediately below is Yugeta-yama, and Kushigamine is peak to left.

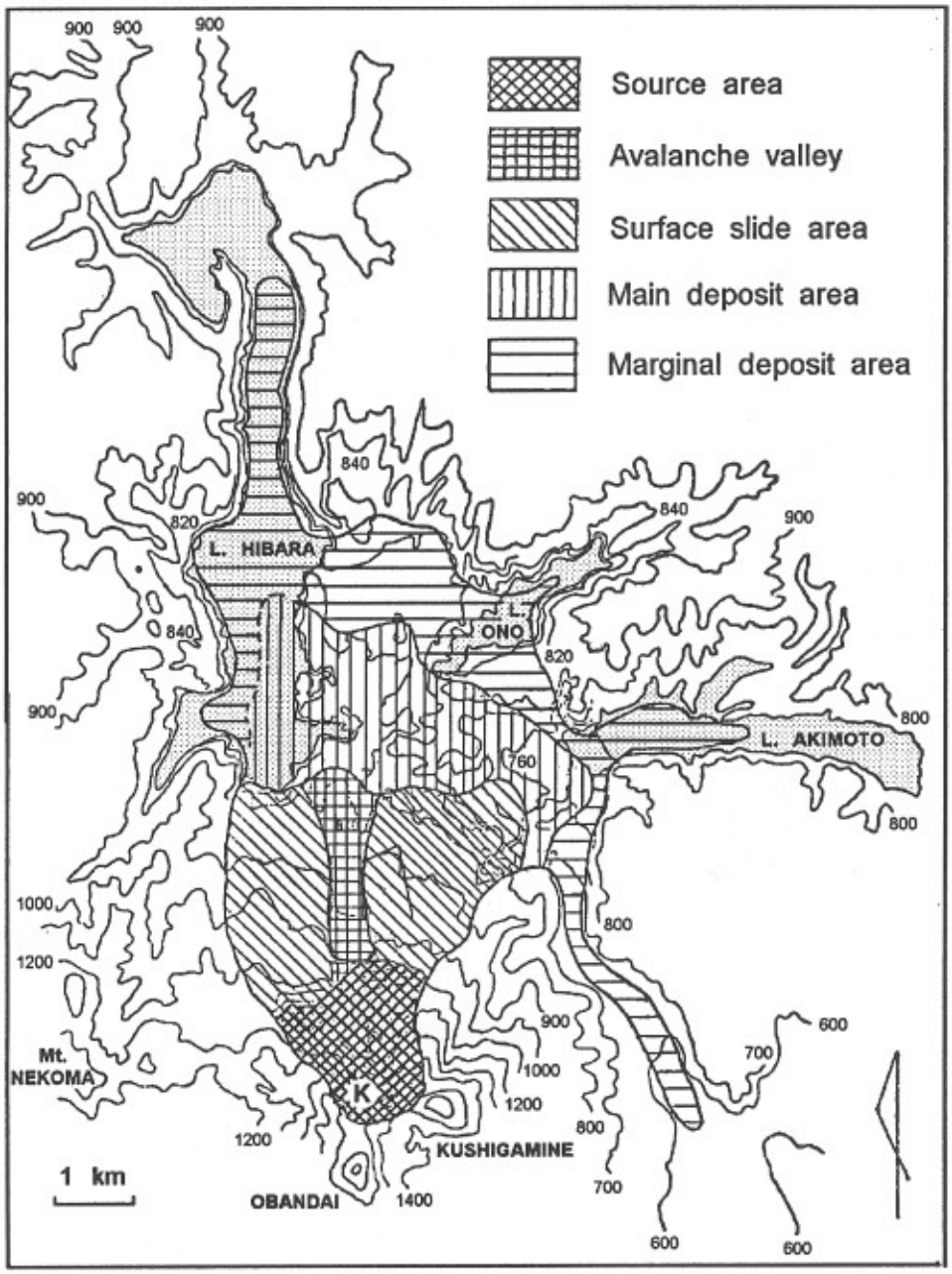

Figure 12. Map of Bandai 1888 debris-avalanche deposit, modified from Nakamura (1978), showing distal extent of deposit now beneath lake waters (stippled areas) from Sekiya and Kikuchi (1889). K marks prefailure location of Kobandai peak.

Obandai, Kushigamine, and Kobandai volcanoes, and failure occurred at the unbuttressed north side of Kobandai (Fig. 12). Surface loading of a sequence of thick lava flows overlying a basal pyroclastic core (Fig. 2) may also have contributed to failure.

Some uncertainty surrounds the timing of the avalanche. Eyewitness accounts and calculations of avalanche velocities suggest that the avalanche occurred at the time of the initial explosions (Sekiya and Kikuchi, 1889; Nakamura, 1978), but Yonechi (1987) interpreted photographs from the southwest, apparently showing Kobandai still standing 1.5 h after the onset of the eruption, to indicate that the avalanche occurred at an undetermined time later on July 15. A sketch by Sekiya and Kikuchi (1889) from the same angle four weeks after the eruption, however, also shows a peak of roughly the same size and location as on the photograph. This peak is thus unlikely to be Kobandai, which would already have been removed by the avalanche, but a subsidiary peak of Kobandai, Yugeta-yama (Figs. 11 and 13), that was later subdued by slumping of the crater rim.

Major slope failures had occurred previously at least three times at Bandai. The largest, ca. 70 ka, produced a 4 km^3 avalanche that traveled 25 km to the southwest (Inokuchi, 1988). Failure again occurred in the same direction when a composite cone

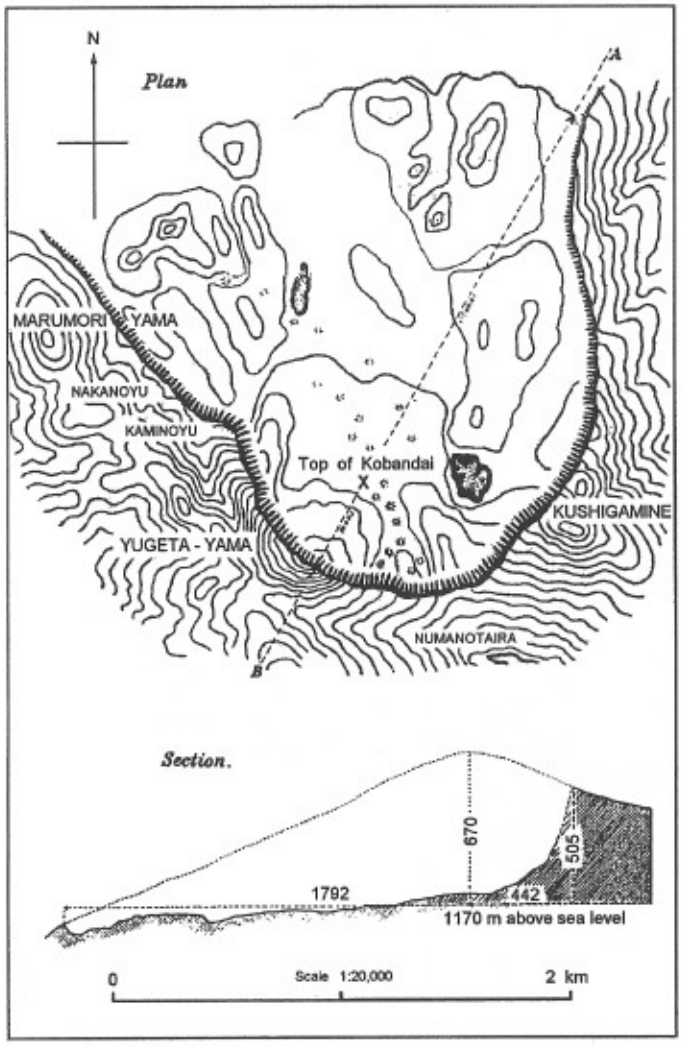

Figure 13. Map and cross-sectional view of 1888 Bandai slope-failure source area (Sekiya and Kikuchi, 1889)

constructed within the earlier collapse scarp failed. Small-scale toreva blocks are present near the source of a younger third avalanche down Biwa-sawa valley on the east side. The source areas of all four slope failures are still visible, although the first two are largely filled by postcollapse reconstruction.

Unzen, 1792

In contrast to the 1980 Mount St. Helens and 1888 Bandai slope failures, the 1792 collapse of the dacitic Mayu-yama lava dome at the Unzen volcanic complex, Japan's most severe volcanic disaster, was not accompanied by explosive eruptions. Although phreatic explosions had often been considered to have triggered the Mayu-yama (Mae-yama) collapse, Katayama (1974) documented that no eruptions occurred at Mayu-yama. Katayama noted the lengthy descriptions of an eruption at the neighboring volcano of Fugen-dake and considered it inconceivable that residents would not have mentioned eruptive phenomena closer at Mayu-yama.

Unusually detailed historical records provide insights into the collapse and events leading up to it. An earthquake swarm at the western end of the Shimabara Peninsula beginning November 3, 1791, reached its peak in the middle of November, then declined. Audible detonations in mid-January, 1792, preceded explosive activity that began about February 10 at Fugen-dake, 5 km west of Mayu-yama and the location of the recent 1990–1994 eruption (Ogawa and Homma, 1926; Katayama, 1974). Beginning on March 1, a 0.11 km^3 lava flow was extruded from two vents on the northeast flank that eventually traveled 2.5 km, overrunning one hamlet (Fig. 14). On April 21, more than 300 felt earthquakes formed fissures to 1 km long and caused extensive damage in the

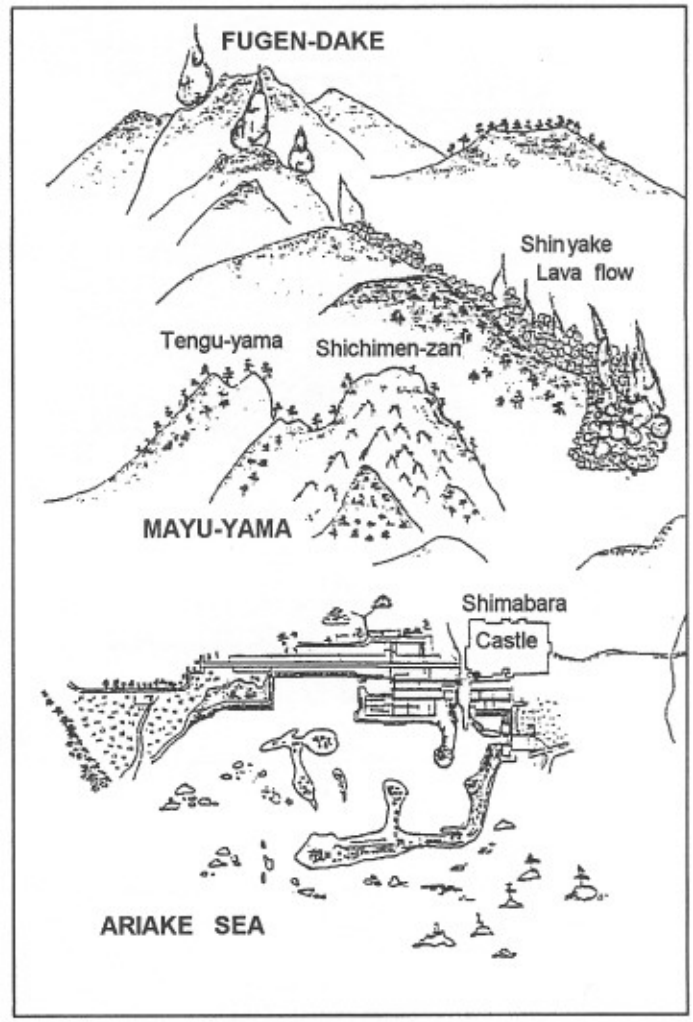

Figure 14. Contemporary sketch of part of Unzen volcanic complex from east showing Tengu-yama (southern peak of Mayu-yama lava dome) prior to edifice failure. Fugen-dake, smoke columns from northeast flank vents, and 1792 lava flow form background. Foreground island hummocks are from pre-1792 debris avalanche. After Noguchi and Ono (1986).

coastal town of Shimabara. Loud detonations sounding to residents like guns from a Dutch frigate came from Mayu-yama, and rockfall produced dust clouds that at times obscured the mountain from Shimabara. Fear of a landslide prompted most of the residents to flee to the north, abandoning their homes. On April 29, part of the lava dome slowly slid 200 m eastward. By the middle of May, however, seismicity had subsided, and residents returned to their homes.

At 8 p.m. on May 21, two intense earthquakes occurred, and 0.34 km^3 of Tengu-yama, the southern of the two lava domes forming Mayu-yama, failed to the east; an avalanche was produced that swept into the Ariake Sea, extending the shoreline by almost 1 km and forming the Tsukumo-shima (Ninety-nine Islands). The avalanche passed south of the main part of Shimabara, overrunning two outlying villages. About 80% of the avalanche entered the sea (Fig. 15), filling up Shimabara harbor and producing a tsunami with three major wave crests that swept over the most populated portion of the town and devastated a 76 km stretch of the Shimabara Peninsula coastline, causing 9528 fatalities. The tsunami traveled 20 km across the Ariake Sea, resulting in another 4996 fatalities in Higo and Amakusa provinces. This volcanogenic tsunami, second in devastation only to the 1883 Krakatau tsunami, caused >14 500 fatalities, injured another 1500, and swept away nearly 6000 houses and 1600 boats, along with 756 cattle and horses.

Bathymetric surveys reveal the submarine extent of the avalanche, which covers ~15 km^2 and traveled 6.5 km from Mayu-yama (Fig. 16). The submarine part of the debris avalanche displays morphological features typical of subaerial debris-avalanche deposits. The dominant orientation of avalanche hummocks changes from radial in the subaerial part to transverse in the distal submarine segment, where ridges as long as several kilometers are common.

The immediate trigger of the avalanche appears to have been the earthquakes of May 21, but elevated pore pressures within the edifice set the stage for collapse. Ota (1973) proposed that failure was due to saturation of the volcanic cone by hydrothermal waters preceding movement of magma along an inclined plane from Chijiwa caldera to the west. Progressively shallowing earthquakes migrating eastward ceased after the failure, and large quantities of hot water poured from the scarp in the weeks to follow, forming a pond at the base of the scarp and a lahar that reached the coast.

Sketches made of the Shimabara area prior to the 1792 landslide also show many island hummocks from a previous landslide (Fig. 14). Bathymetry shows an area of hummocky topography and closed depressions extending several kilometers north of the 1792 debris avalanche from this older prehistoric avalanche.

Augustine 1883

Augustine volcano in Cook Inlet, Alaska, has undergone frequent, repetitive slope failure. The repeat rate of edifice collapse on this small, 1250-m-high andesitic lava dome complex is the highest currently known at any volcano; at least 11 events were documented during the past 2 k.y. (Begét and Kienle, 1992; Waitt and Begét, 1996). The most recent landslide occurred on October 6, 1883, when the summit of Augustine collapsed (Fig. 17), producing the Burr Point debris avalanche that swept into the sea on the north coast of the island (Siebert et al., 1989, 1995). Much of the proximal portion of the avalanche deposit is covered by postcollapse pyroclastic-flow deposits, but along the

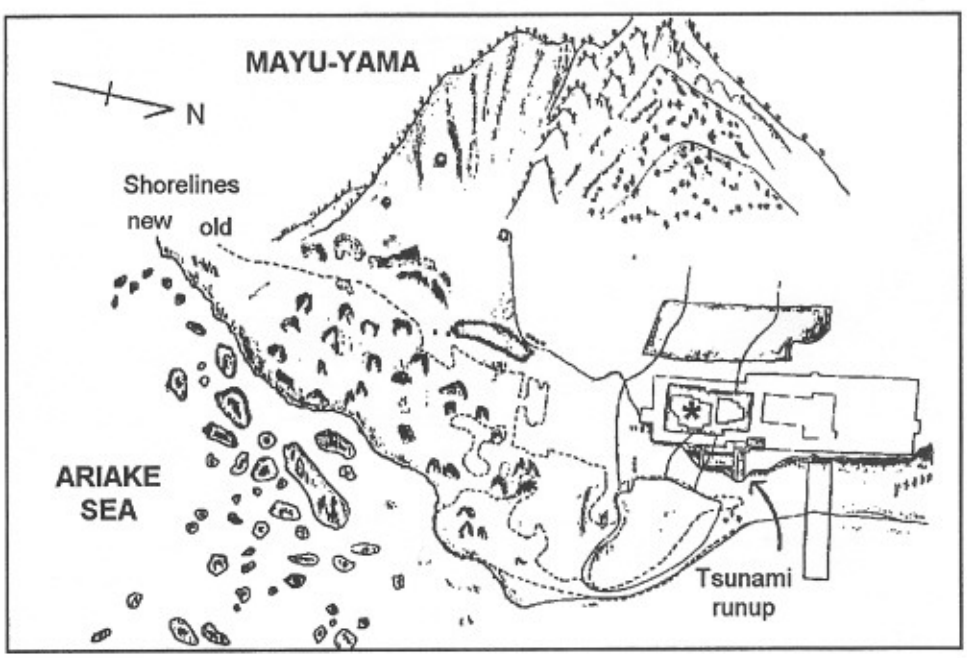

Figure 15. Postcollapse sketch from east showing extended shoreline and newly formed islands from 1792 failure of Mayu-yama. Tsunami runup reached Otemon gate at southeast corner of Shimabara castle (asterisk). After Katayama (1974).

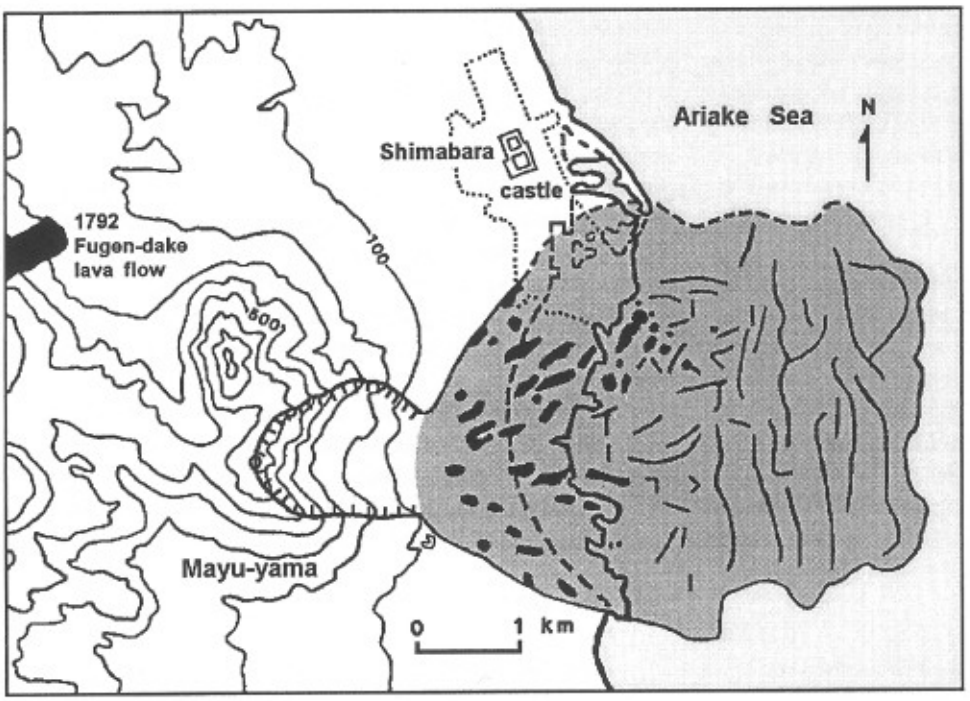

Figure 16. 1792 Unzen avalanche deposit (shaded area). Avalanche source area at Mayu-yama is shown by hachures. Subaerial avalanche hummocks (black areas) extend radially away from Mayu-yama and form islands in Ariake Sea; lines show largely transverse orientation of submarine avalanche-deposit ridges, resulting from deceleration of avalanche as it entered sea (Siebert et al., 1995). Heavy solid line marks modern shoreline; dashed line to west is approximate location of pre-1792 shoreline (after Ota, 1969). Submarine extent of avalanche is from bathymetry of Geographical Survey Institute (1982). Dotted line is modern boundary of Shimabara City. Contour interval is 100 m.

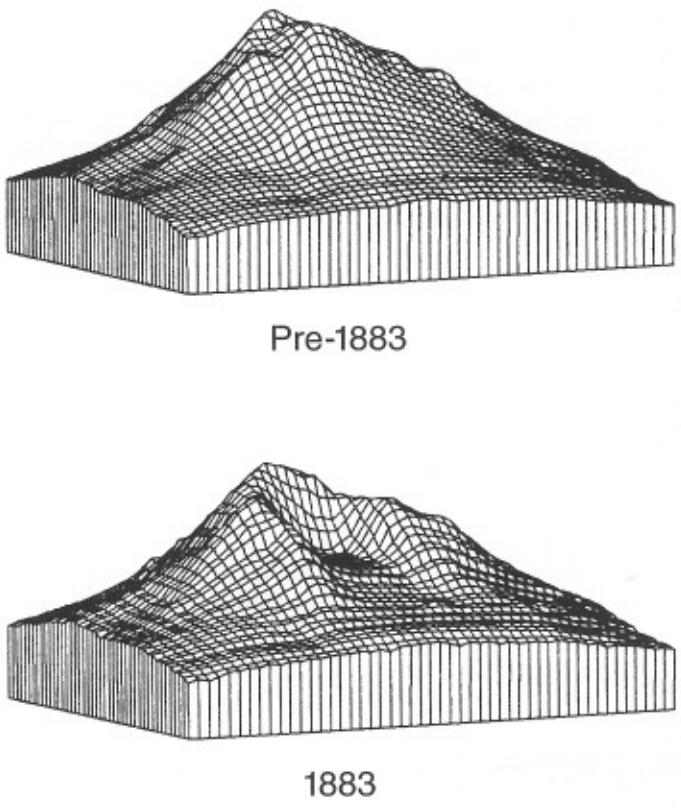

Figure 17. Low-angle aerial oblique perspectives of Augustine from northeast inferred from precollapse sketch and postcollapse photograph. Volume differential is 0.25 km^3 (Siebert et al., 1989). Base of perspective blocks is at sea level, summit is ~1200 m, width of failure scarp is just <1 km.

coast the avalanche deposit forms abundant hummocks and small islands to ~10 m in height. Large fragments of the summit lava domes with a maximum exposed dimension of 25 m traveled as far as the present shoreline. Bathymetry and the location of the still-visible pre-1883 shoreline (at about the 200 ft contour in Fig. 18) indicate that the avalanche traveled ~4 km beyond the 1883 coast. Like the 1792 Unzen deposit, the submarine portion of the Burr Point avalanche deposit (including areas now above sea level) displays a series of transverse ridges, attributed to deceleration of the avalanche as it entered the sea (Siebert et al., 1995).

Magmatic eruptions following the collapse produced pyroclastic flows and surges that reached the new coastline, air-fall tephra that extended across Cook Inlet, and a lava dome that filled much of the landslide scarp. A north flank lava flow that appears to originate within the 1883 landslide scarp is considered to have formed in this eruption (Siebert et al., 1989, 1995), although Waitt and Begét (1996) inferred a slightly earlier prehistorical date. A tsunami was reported by Davidson (1884) to have caused damage to a village across Cook Inlet.

Structural influences on collapse are less pronounced at Augustine, where volcanism has been concentrated at a single central conduit, and previous collapses have produced subaerial and submarine avalanche deposits that ring the island (Begét and Kienle, 1992). The West Island debris avalanche (Fig. 7), ca. 367 ^{14}C yr B.P., was among the largest (~0.5 km^3). It traveled 11 km, forming West Island, and was accompanied by a small lateral blast (Siebert et al., 1989, 1995). The high edifice failure rate at Augustine has produced a volcaniclastic apron surrounding the volcano several times the volume of the edifice. An equilibrium between volcano growth and destruction at rates of 1–3 × 10^6 m^3/yr

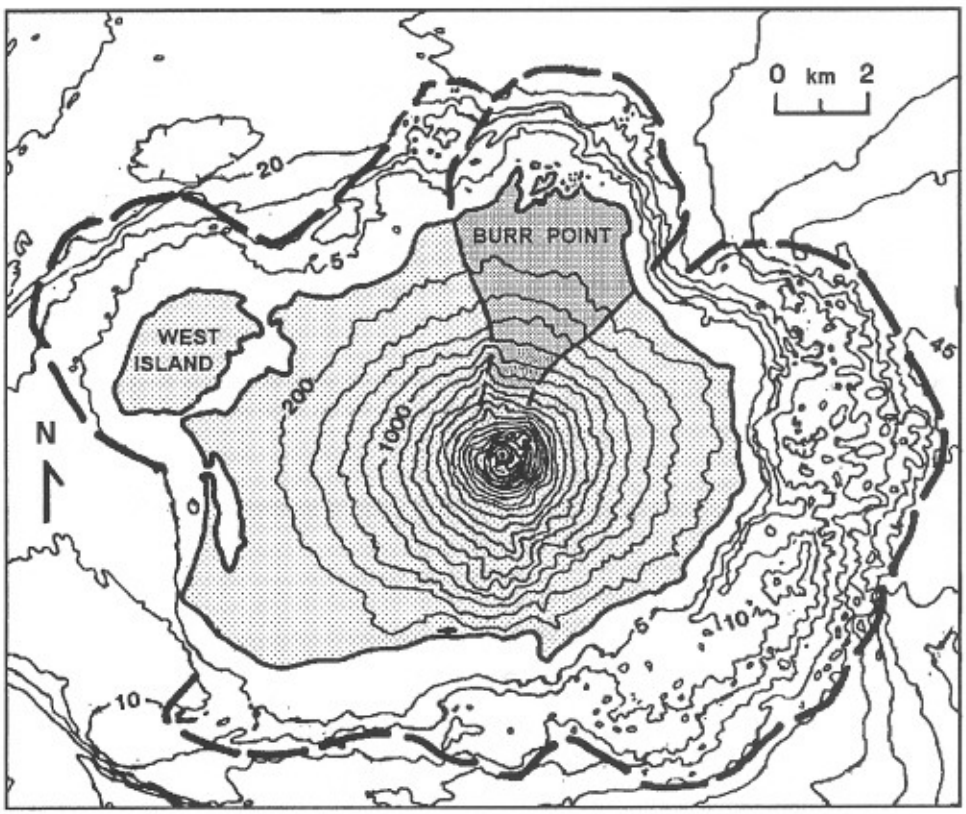

Figure 18. Map of Augustine Island showing areal extent of Burr Point debris-avalanche deposit (darker stipple pattern; much of proximal area is overlain by pyroclastic-flow deposits). Dashed lines mark submarine terminus of this and other debris-avalanche deposits. Contour interval is 200 ft (61 m).

has existed over the past 2 k.y. (Begét and Kienle, 1992; Siebert et al., 1995).

Socompa

Volcán Socompa, a 6051 m stratovolcano in the central Andes straddling the Chile-Argentina border, collapsed ~7200 yr ago, producing a large debris avalanche that swept 37 km to the northwest (Fig. 19). Long-term studies by Peter Francis and colleagues over the past decade have made this remote avalanche deposit one of the better known. Although ground access to part of the deposit is facilitated by a railroad line, the scale of the deposit has necessitated extensive use of remote-sensing applications to characterize it (Francis et al., 1985; Francis and Self, 1987; Wadge et al., 1995).

Collapse involved a 70° sector of the northwest side of the andesitic-dacitic composite volcano, leaving a triangular-shaped source area 10 km wide at the breach. The Socompa collapse is unusual in that a large component of the failure mass (estimated as large as 44 km^3 by Wadge et al., 1995) remained within the source area in the form of massive rotated toreva and other blocks that did not disaggregate. The detachment surface truncated portions of the basement beneath the composite cone (Fig. 20), as seen from the inclusion of pre-Socompa mudflow and pyroclastic-flow deposits and Tertiary volcaniclastic gravels within the debris-avalanche deposit. Gravitational loading of thick dacitic and andesitic lava flows and domes over a pyroclastic-rich basement substrate may have contributed to structural failure; the presence of an associated explosive deposit and fresh, glassy dacite blocks with breadcrust jointing within the avalanche deposit also points to the role of magma that was present within the edifice at the time of collapse.

Originating from an arid-region volcano that was not extensively glaciated, the Socompa avalanche was substantially drier than the 1980 Mount St. Helens and many other debris avalanches. This lack of water is reflected in the absence at Socompa of the bimodal block facies and mixed facies component common at many other avalanche deposits and by the absence of a distal mudflow facies. The prominent lateral levees that exceed 40 m in height on the northern and western distal margins and the relative thickness of the deposit in unconfined terrain, estimated to be 60 m along the axis of the deposit to its distal end, are also evidence of the relatively dry character of the Socompa avalanche.

Failure, as at Mount St. Helens, was retrogressive, involving headward migration of multiple slide blocks. A prominent 50-m-high scarp cutting diagonally across the deposit results from the overriding of earlier deposited material by a later avalanche lobe (Wadge et al., 1995). Modeling of the centroids of prefailure and displaced masses show a potential energy loss of 3.8×10^{17} J, five times that at Mount St. Helens. Some components of the avalanche with the least potential energy traveled the farthest, suggesting a momentum transfer from the rear to front of the failed mass (Wadge et al., 1995).

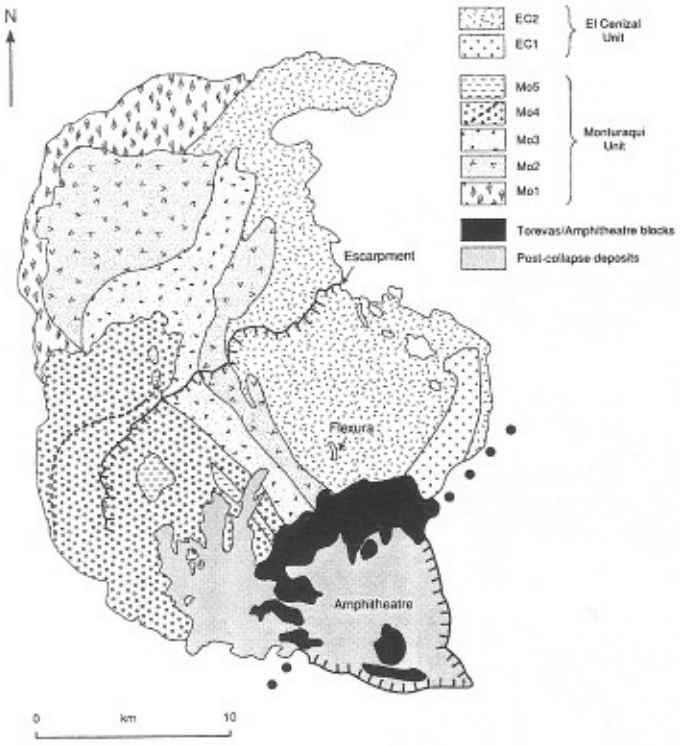

Figure 19. Map showing subunits of Socompa debris-avalanche deposit and toreva blocks (black) that slid to base of source area without disaggregating (Wadge et al., 1995).

Magmatic eruptions accompanied the collapse, including a thin pyroclastic flow that extended beyond the western and southern margins of the avalanche deposit (Francis and Wells, 1988). Copious dacitic lava flows have subsequently filled much of the source area.

Shasta

Earth's largest documented continental Quaternary debris avalanche occurred ca. 300–380 ka, when collapse of an ancestral Mount Shasta volcano in the southern Cascade Range of California produced an avalanche that covered a 675 km^2 area with a volume of at least 46 km^3 (Crandell, 1989). The avalanche traveled tens of kilometers over Shasta Valley slopes of <1° for a total distance of ~50 km from its source (Fig. 21), producing a topography dominated by hundreds of small hills and ridges, decreasing in size and number to the northwest, that rise above a flat valley floor. This topography had previously been variously interpreted as individual volcanic vents, moraines, or stream-dissected volcanics, but it drew the attention of geologists who had worked on the Mount St. Helens avalanche deposit and recognized the landslide origin of the Shasta Valley deposits (Crandell et al., 1984). Individual hummocks are of circular to irregular shape and range to 175 m in height. Sinuous ridges, often oriented transverse to transport direction, are present, the largest reaching a length of 8–9 km and a maximum height of 210 m. In the central part of Shasta Valley the avalanche was diverted around a number of Tertiary hills.

Block facies material includes lava-flow remnants and extensive stratigraphically upright segments of pyroclastic-flow, lahar, and air-fall deposits, sometimes with intervening soil horizons, offset by normal faults. Individual blocks range to hundreds of meters in length. The mean size (220 m) of block facies segments that consisted of pyroclastic materials was twice the size of those composed of massive lava flow remnants, suggesting that stress within the transported pyroclastic blocks was accommodated by deformation rather than brittle fracturing (Ui and Glicken, 1986). The more fluid mixed facies material drapes many hummocks and fills broad interhummock areas (Fig. 22), distally forming veneers on valley walls. Proximal portions of the mixed facies material predominantly contain angular to subangular pebbles of

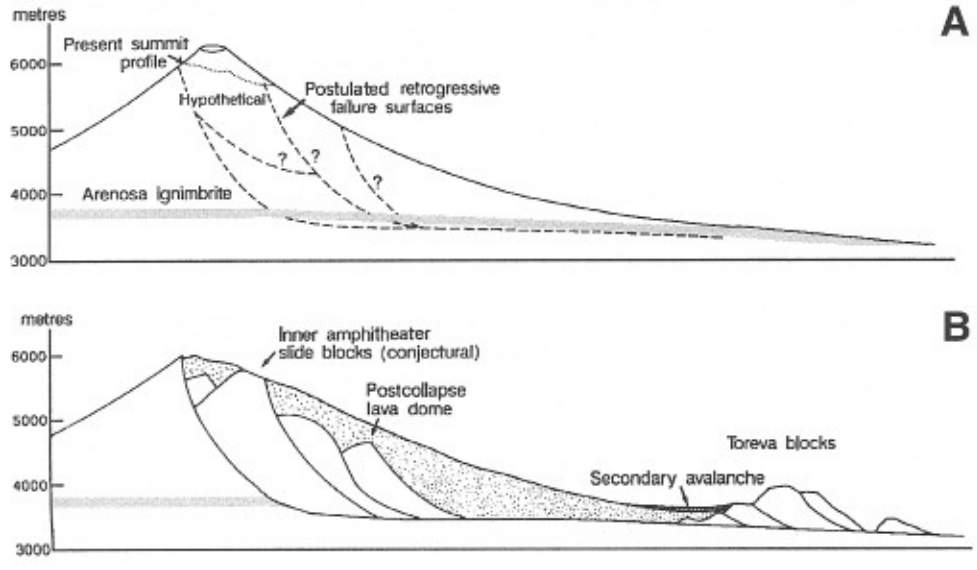

Figure 20. Cross-sectional profiles of Socompa before (A) and after (B) collapse (after Wadge et al., 1995). Shaded area in lower view is present profile.

Mount Shasta lithologies; more distal portions contain progressively increasing amounts of rounded to subrounded non-Shasta rocks scoured by and incorporated in the avalanche. Despite the age of the deposit, its surface is relatively undissected.

The Shasta avalanche had a higher water content than the Mount St. Helens avalanche. The mixed facies was wetter (22.5% water in one sample measured) and is considered to have partially drained away after more coherent block facies material came to a rest (Crandell, 1989). Boulders of Mount Shasta lithologies are found as much as 100 m above the surface of the avalanche deposit and represent a lag deposit formed when the still-fluid mixed facies material drained away. No evidence was found of contemporaneous volcanic eruptive activity. Failure was subperpendicular to a north-south–trending fissure that fed a series of modern Mount Shasta cinder cones and lava domes; however, these and other Quaternary eruptions of Shasta have buried almost all remnants of the avalanche source area, obscuring evidence of prefailure structures.

Raung

Collapse of Raung volcano at the eastern end of Java produced Indonesia's largest known debris avalanche. The avalanche deposit was first recognized by Neumann van Padang (1939), who described a large hummocky deposit that extended 60 km from its source on Gunung Gadung, a composite volcano on the east flank of 3332-m-high Raung volcano, 4 km from the Raung caldera rim. Recent work has traced the deposit to 79 km from the source headwall (Siebert et al., 1996). The deposit covers an area of >1000 km^2 east and southeast of Gunung Gadung, filling the broad valley between the Iyang-Argapura volcanic complex and Tertiary mountains that extend to the coast (Fig. 23). Failure direction to the east was influenced by the buttressing effect of Gunung Raung immediately to the west.

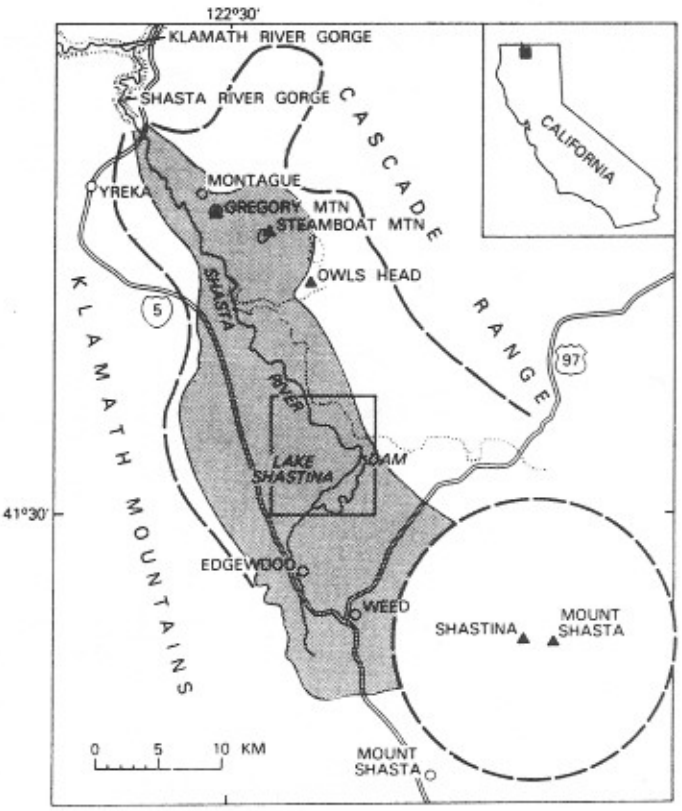

Figure 21. Map of Shasta Valley debris-avalanche deposit (Crandell et al., 1984).

The proximal area extending 30 km from the breached source area toward the city of Jember contains abundant hummocks to ~75 m height consisting of segments of lava flows in varying stages of fragmentation and thick sequences of slightly indurated, flat-lying to steeply dipping tephra layers usually several tens of

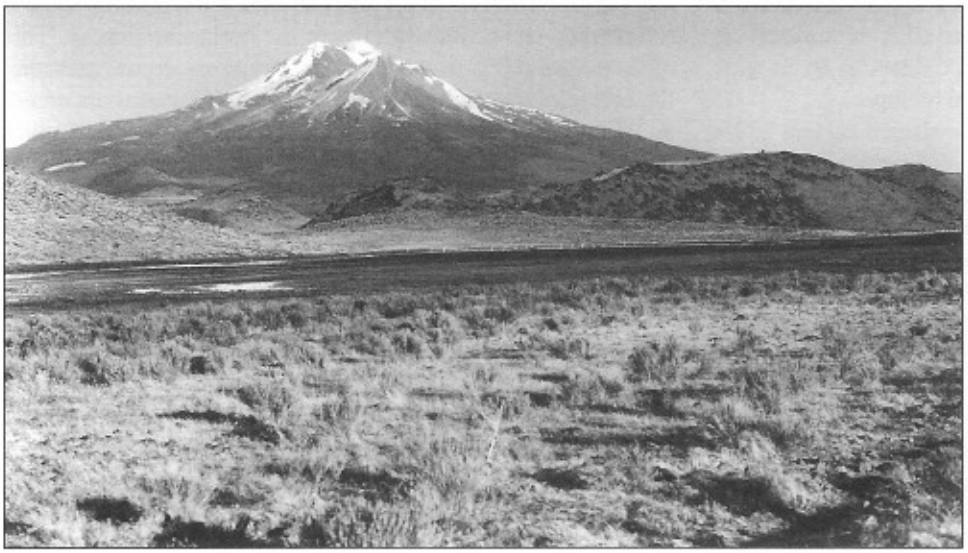

Figure 22. Block facies hills of Shasta Valley debris-avalanche deposit (Crandell, 1989) viewed from 40 km northwest of Mount Shasta, with mixed facies material in foreground.

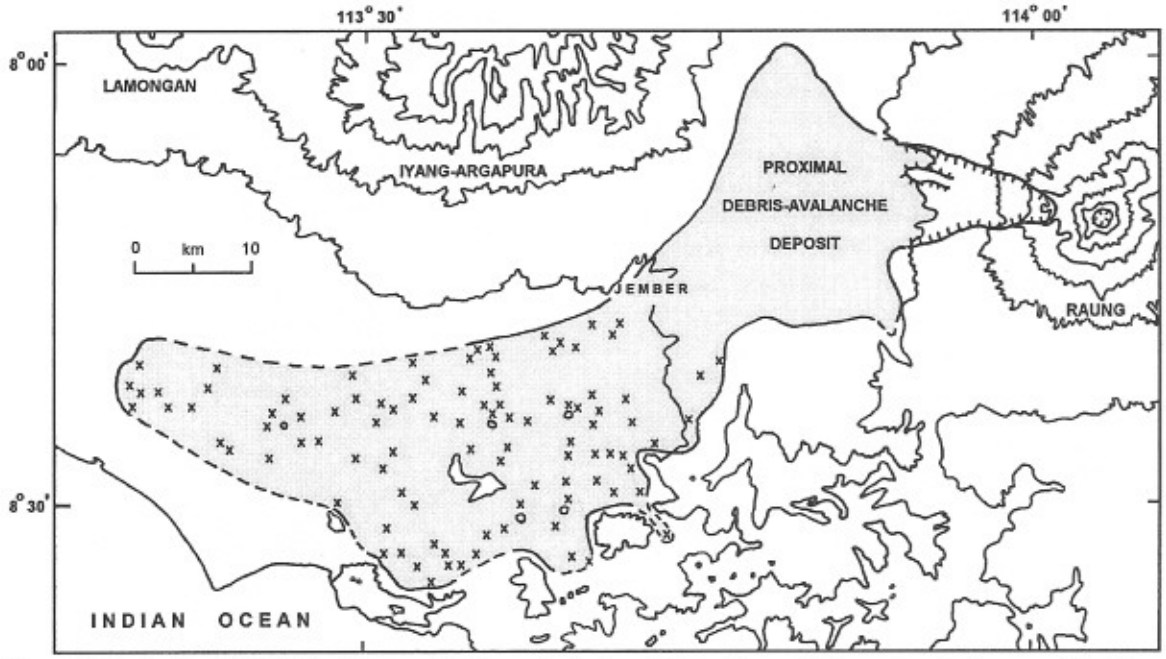

Figure 23. Preliminary 1:250000-scale map of debris-avalanche deposit from Gunung Gadung. Proximal area contains abundant closely spaced hummocks; x symbols mark sparser hummocks and hummock clusters in distal area southeast of city of Jember. Irregular contours and small circles in distal area outline six Tertiary hill outliers. Contour interval is 500 m; addition of 100 m contour is to help delineate Miocene hills south of avalanche deposit. Hachures outline Gunung Gadung avalanche caldera and summit caldera of Raung volcano; hachured area within avalanche scarp is probable remnant of prefailure surface, Gunung Malang.

centimeters thick (Fig. 8). Mixed facies and/or lahar facies material containing scattered subangular clasts in a finer matrix dominates in the distal portions of the deposit, deflected to the south by the Iyang-Argapura complex. Distal hummocks are smaller (usually <20 m high), fewer, more widely scattered, and consist primarily of the bedded tephra layers found in the proximal area. Hummocks occur to the extreme distal end of the deposit (Fig. 23), which diverted local drainages. The avalanche flowed around six Tertiary hill outliers in the flat-lying distal area. Distal hummocks are often preferentially stranded adjacent to these hills, which reversed the local gradient. Clastic dikes, to >1 m wide, were observed in both proximal and distal hummocks.

The avalanche left a large horseshoe-shaped caldera 13 km long and 8.5 km wide at the breach (Fig. 24), reducing the height of Gunung Gadung from an estimated 2800–3000 m to 2399 m. Gunung Malang, a steep-sided, flat-topped 1-km-wide ridge parallel to the caldera walls, is composed of lavas similar in altitude and lithology to those forming the caldera walls, and is considered to be a remnant of the prefailure edifice that either moved only a short distance (Neumann van Padang, 1939), or remained in place when the failure plane bifurcated. Proximal avalanche material restricted drainage, forming ephemeral lakes on either side of Gunung Malang within the avalanche caldera. Restoration of contours, assuming that the Gunung Gadung failure plane (Fig. 25) had the same slope angle as at the morphologically similar Galunggung slope failure in western Java, produces an estimated failure volume of 20 km^3. Dilation of avalanche material during emplacement is typically 25% (Siebert et al., 1987); this would result in an estimated deposit volume at Raung of 25 km^3.

Although unequivocal new magmatic material was not observed in the avalanche deposit, associated explosive activity, which could have left deposits that underlie the avalanche deposit, is not excluded. A thin unit near the top of portions of some hummocks that bears some resemblance to a lateral-blast deposit (H. Glicken, 1990, personal commun.) was not seen in interhummock sections or outside the avalanche deposit. This raises the possibility that it was an allochthonous deposit predating the collapse, although the origin of this unit remains uncertain. A widespread three-layer pumiceous air-fall unit and other tephras overlie the proximal part of the avalanche deposit, but intervening soil layers indicate that they postdate the avalanche. Postcollapse eruptions have constructed the Gunung Pajungan stratovolcano within the avalanche caldera to the height of its rim, along with a small cinder cone on its east-northeast flank.

Koolau

The surge of interest in subaerial volcanic landslides following the 1980 Mount St. Helens eruption also led to the recognition of many submarine landslide deposits from oceanic shield volcanoes. Since 1980, dozens of massive submarine landslides of late Tertiary to Pleistocene age have been recognized in the

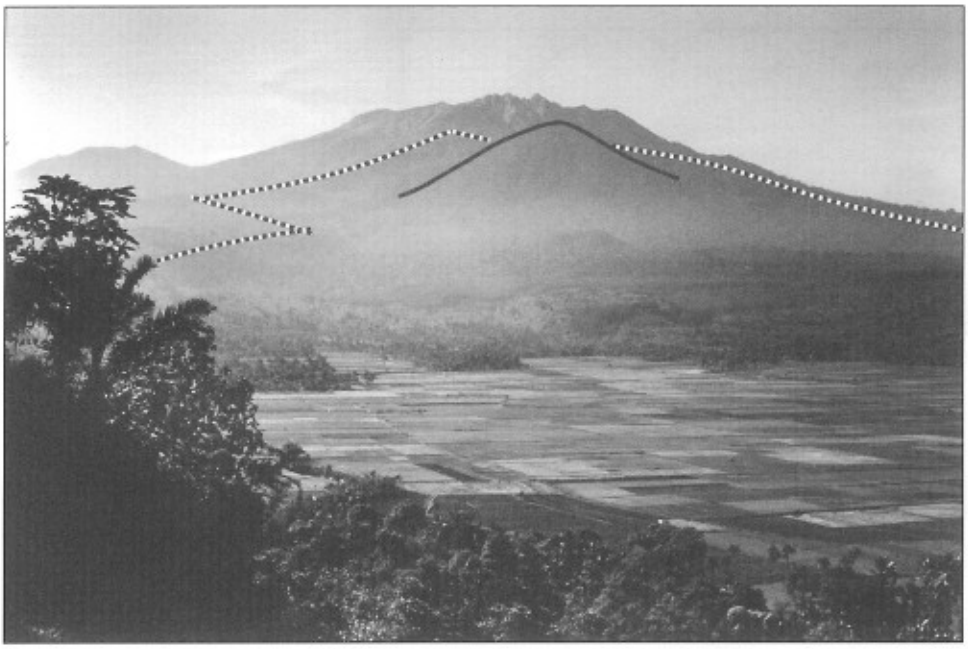

Figure 24. Failure scarp (dashed line) of landslide from Gunung Gadung is 8.5 km wide in photo. Postcollapse eruptions have constructed Gunung Pajungan (solid line) near failure headwall. Raung volcano is in background.

Hawaiian Islands (Fig. 26; Moore et al., 1994), and this process is relatively common at other oceanic volcanoes (Holcomb and Searle, 1991). These landslides are massive in scale, one to two orders of magnitude more voluminous than the largest Quaternary avalanches from continental volcanoes. Rapid gravitational failures producing long-runout debris avalanches and long-term slower failures creating deep-seated slumps are observed at oceanic and coastal volcanoes (Moore et al., 1994; McGuire, 1996).

The Nuuanu debris avalanche traveled 230 km from its source on Koolau volcano on the Hawaiian island of Oahu, covering an area of 23 000 km^2. Its estimated volume is ~5000 km^3 (Moore et al., 1989). The avalanche, later partially overlapped by an avalanche from Molokai volcano, crossed the axis of the Hawaiian Deep, and traveled an additional 140 km up a gentle slope of 300 m (Fig. 26). A large number of giant tilted blocks (the largest 30 × 17 km wide and 1.8 km high) slid 50 km or more and may be analogous to the toreva blocks described at Socompa volcano. Scattered hummocks ranging to 1 km in width are found at the distal end of the deposit. The landslide source area is visible in bathymetry and suggests removal of 0.7–1.1 km of material. A 40-km-long dike swarm on Koolau volcano at the head of the scarp is oriented normal to the failure direction and may have influenced collapse direction. A common feature of source areas of submarine failures is the development of deeply incised canyons formed by rapid subaerial erosion of oversteepened, recently stripped slopes that were later submerged by regional subsidence (Moore et al., 1994).

The morphology of these massive submarine avalanche deposits is comparable to those of subaerial avalanches, suggesting that the submarine avalanches also involve rapid flow, with attendant tsunami hazard (Moore et al., 1994). The failure of low-angle shield volcanoes with slopes <10° likely involves mechanisms in addition to those at subaerial stratovolcanoes. Ellsworth and Voight (1995) noted the failure-triggering potential of excessive pore pressures produced by laterally extensive dike intrusions. Large masses of cumulate olivine at the base of the volcanic pile, where temperature-pressure conditions produce a flowing mass with a rheology similar to ice, are considered to contribute to the slope instability of oceanic shield volcanoes (Clague and Denlinger, 1994). Recent studies have related magmatic-head pressure to Kilauea south flank instability (Borgia, 1994; Dvorak, 1994; Iverson, 1995; Denlinger and Okubo, 1995).

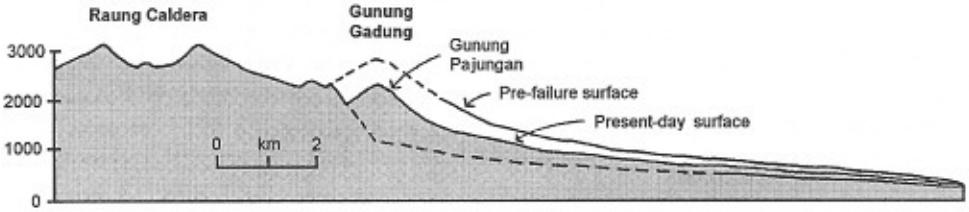

Figure 25. Cross-sectional view of Gunung Gadung avalanche caldera showing inferred profiles before and after collapse; shaded area is current profile.

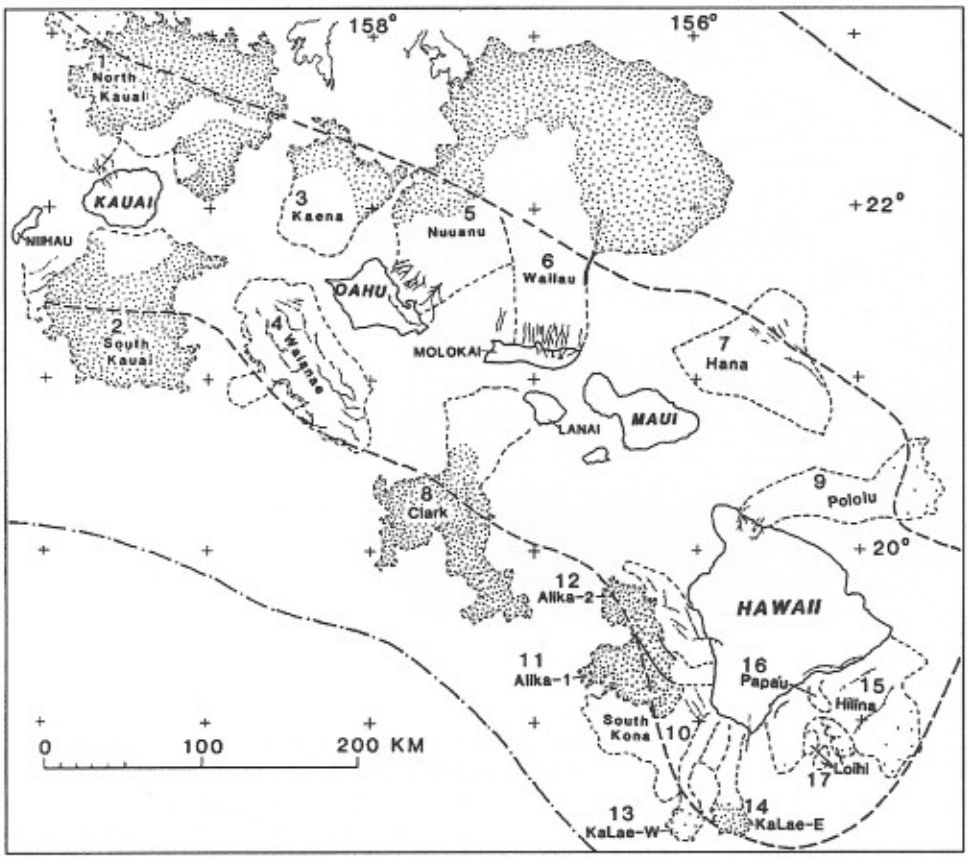

Figure 26. Debris avalanches along southeastern Hawaiian Ridge (Moore et al., 1989). Dotted areas show hummock groups, thin lines near source areas are submarine and related subaerial canyons, and thin hachured lines are scarps. Heavy dark line marks axis of Hawaiian Deep, dash-dotted line marks crest of Hawaiian Arch.

HAZARDS

Large volcanic landslides can be among the most hazardous events at volcanoes. Although the repeat rate is low at individual volcanoes, their great mobility distributes large volumes of material great distances beyond the volcano at rates that preclude effective hazard mitigation after they occur. Hazard risk assessment at volcanoes has focused on the estimation of likely travel distances of future avalanches. This has been done using procedures including the use of empirical data from many avalanches to characterize fall height/travel distance ratios, the scale modeling of analogous physical substances, or the theoretical dynamic modeling of flow behavior. A rough first approximation of the mobility of large debris avalanches can be empirically characterized by the ratio of height to runout distance (*H*/*L*) of avalanche deposits (Ui, 1983; Voight et al., 1983; Schuster and Crandell, 1984; Siebert, 1984; Ui et al., 1986b; Siebert et al., 1987; Francis and Wells, 1988; Crandell, 1989; Hayashi and Self, 1992). The effect of volume on travel distance (Fig. 4) can be considered by using characteristic *H*/*L* ratios of avalanches in different size classes, which can be related to edifice size (Siebert, 1996). Energy-line calculations such as these overestimate velocity and underestimate travel time and do not consider rheological and other factors influencing movement. More complex calculations that more closely factor in emplacement mechanisms have successfully been applied retrospectively to the Mount St. Helens avalanche (McEwen and Malin, 1989; Sousa and Voight, 1991, 1995). However, difficulties in precisely anticipating the potential volume, rheology, and other model parameters make determining the precise runouts of future avalanches problematical.

Hazards of landslides at volcanoes can be exacerbated by eruptions that accompany, or are triggered by, collapse of the edifice. Associated eruptive activity can range from mild to moderate phreatic explosions to major Plinian eruptions that deposit pumice and ash over wide areas. In some cases, powerful lateral explosions resulting from the sudden depressurization of hydrothermal-magmatic systems by removal of edifice slide blocks, such as occurred at Bezymianny volcano in Kamchatka in 1956 and Mount St. Helens in 1980, can devastate hundreds of square kilometers. Relatively few directed-blast deposits of this type have been described, and many collapse events with associated magmatic eruptions have not produced lateral explosions. Lateral blasts on the scale of Mount St. Helens (Hoblitt et al., 1981; Moore and Sisson, 1981; Waitt, 1981; Fisher et al., 1987) have to date been documented in association with avalanches only at Bezymianny (Gorshkov, 1959; Bogoyavlenskaya et al., 1985; Belousov, 1996) and possibly at Taunshits volcano in Kamchatka (Melekestsev et al., 1990), Guagua Pichincha volcano in Ecuador (Barberi et al.,

1992), and Popocatépetl in Mexico (Siebe et al., 1995). Smaller directed blasts have been described at Soufrière Guadeloupe (Boudon et al., 1984), Augustine (Siebert et al., 1989), Cerro Quemado (Conway et al., 1992), Komaga-take (Yoshimoto and Ui, 1997), and possibly Bandai (Glicken and Nakamura, 1988).

The occurrence of this type of laterally directed explosion is related to the degree of coincidence of landsliding and explosions; the landslides also serve to deflect the explosions and contribute material to the ensuing horizontally traveling pyroclastic density currents (Siebert, 1996). Deposits from pyroclastic surges and pumiceous pyroclastic flows, both texturally distinct from lateral-blast deposits, have been noted overlying debris-avalanche deposits at many volcanoes and often result from open-vent processes that follow removal of the landslide mass.

Lahars form in relationship to debris avalanches over a wide time frame. Lahars can form directly by transformation from debris avalanches during emplacement (Pierson, 1985; Scott et al., 1995), from dewatering of debris-avalanche deposits shortly after emplacement (Fairchild, 1987), or from breakouts of avalanche-dammed lakes weeks to many months after the avalanche. Although these lahars are of lower velocity than debris avalanches or lateral blasts and are more constrained by topography, they can travel significantly farther, and cover broad lowland areas, with great impact. Inundation levels within confined valleys of large-scale lahars resulting from sector collapse may reach 100 m or more above the valley-floor deposits they leave (Scott and Vallance, 1995).

Another indirect hazard of volcanic landslides is tsunamis, which result from the impact of debris avalanches into the sea or inland lakes. Their effect is considerable; nearly 80% of the ~25 000 historical fatalities from large volcanic landslides derived from tsunamis (Siebert, 1996). In addition to the Unzen devastation in 1792, tsunamis were the principal cause of fatalities at five other historical slope failure events. Kienle et al. (1987) and Smith and Shepherd (1996) modeled potential regional effects of tsunamis from volcanic landslides, which can affect areas several hundred kilometers from the volcano.

Although only a small fraction of the potential energy of a landslide is converted into tsunami energy, nearshore wave amplification has produced runups in historical time of as far as a few tens of meters from volcanic landslides (Siebert et al., 1987). Modeling of tsunami propagation is complicated by difficulties in accurately estimating the initial wave displacement and by the complexity of nearshore runup calculations. Nearshore wave heights can range widely due to variable wave amplification influenced by local bathymetry, resonance effects, and other factors (Kowalik and Murty, 1992).

SUMMARY

Following renewed focus on volcanic mass movements after the 1980 eruption of Mount St. Helens, massive volcanic landslides have been reported at more than 350 Quaternary volcanoes. Volcanic landslides are more mobile (*H/L* 0.04–0.20) than nonvolcanic landslides. Their deposits are morphologically and texturally similar to those of many nonvolcanic landslides, but are typically substantially more voluminous (10^{-1} to $>10^{3}$ km^3) and have traveled longer distances (often tens of kilometers to >100 km). Landslides may occur at volcanoes in the absence of eruptions, but they often trigger, or are accompanied by, large explosive eruptions that may include devastating lateral blasts.

Successful hazard mitigation for large volcanic landslides requires prefailure evacuation of areas likely to be affected. The high mobility of volcanic debris avalanches places large areas of dense population within risk. However, the low recurrence rate of avalanches at individual volcanoes often effectively precludes hazard zoning that restricts occupancy of potentially affected areas. The difficulty of anticipating whether edifice failure will occur during a given eruption (or in the absence of an eruption) can produce severe political and economic problems, even for shorter term hazard mitigation efforts.

ACKNOWLEDGMENTS

Interest in volcanic slope failures has long since expanded to where formal citation of all contributors is not possible, but investigators of many nationalities have advanced understanding of these events. Greg Brooks and Edmund Medley provided helpful comments on this paper in review.

REFERENCES CITED

Adushkin, V.V., Zykov, Y.N., and Fedotov, S.A., 1995, Mechanism of volcanic slope failure: Assessment of potential collapse and debris avalanches at Klyuchevskoi volcano: Volcanology and Seismology, v. 16, p. 667–684.

Barberi, F., Ghigliotti, M., Macedonio, G., Orellana, H., Pareschi, M.T., and Rosi, M., 1992, Volcanic hazard assessment of Guagua Pichincha (Ecuador) based on past behavior and numerical models: Journal of Volcanology and Geothermal Research, v. 49, p. 53–68.

Basset, T., 1996, Histoire éruptive et évaluation des aléas du volcano Acatenango (Guatemala) [Ph.D. thesis]: Terre & Environment, Section des Sciences de la Terre, Université de Genève, v. 3, p. 1–240 and appendixes.

Begét, J.E., and Kienle, J., 1992, Cyclic formation of debris avalanches at Mount St. Augustine volcano, Alaska: Nature, v. 356, p. 701–704.

Belousov, A.B., 1995, The Shiveluch volcanic eruption of 12 November 1964: Explosive eruption provoked by failure of the edifice, *in* Ida, Y., and Voight, B., eds., Models of magmatic processes and volcanic eruptions: Journal of Volcanology and Geothermal Research, v. 66, p. 357–365.

Belousov, A.B., 1996, Deposits of the 30 March 1956 directed blast at Bezymianny volcano, Kamchatka, Russia: Bulletin of Volcanology, v. 57, p. 649–662.

Belousova, M., 1994, Large scale edifice failures and associated explosive eruptions in the history of Shiveluch volcano (Kamchatka): Colima, Mexico, Colima Volcano Fourth International Meeting, Universidad de Colima, Abstracts, p. 63.

Bogoyavlenskaya, G.E., Braitseva, O.A., Melekestsev, I.V., Kiriyanov, V.Y., and Miller, C.D., 1985, Catastrophic eruptions of the directed-blast type at Mount St. Helens, Bezymianny and Shiveluch volcanoes: Journal of Geodynamics, v. 3, p. 189–218.

Borgia, A., 1994, A dynamic basis for volcanic spreading: Journal of Geophysical Research, v. 99, p. 17791–17804.

Boudon, G., Semet, M.P., and Vincent, P.M., 1984, Flank failure-directed blast eruption at Soufrière Guadeloupe, French West Indies: A 3,000-yr-old Mount St. Helens?: Geology, v. 12, p. 350–353.

Bronto, S., 1989, Volcanic geology of Galunggung, West Java, Indonesia [Ph.D. thesis]: University of Canterbury, unpublished, 490 p.

Campbell, C.S., 1989, Self-lubrication for long runout landslides: Journal of Geology, v. 97, p. 653–665.

Campbell, C.S., Cleary, P.W., and Hopkins, M., 1995, Large-scale landslide simulations: Global deformation, velocities and basal friction: Journal of Geophysical Research, v. 100, p. 8267–8283.

Carracedo, J.C., 1996, A simple model for the genesis of large gravitational landslide hazards in the Canary Islands, *in* McGuire, W.J., Jones, A.P., and Neuberg, J., eds., Volcano instability on the earth and other planets: Geological Society [London] Special Publication 110, p. 125–135.

Carrasco-Núñez, G., Vallance, J.W., and Rose, W.I., 1993, A voluminous avalanche-induced lahar from Citlaltepetl volcano, Mexico: Implications for hazard assessment: Journal of Volcanology and Geothermal Research, v. 59, p. 35–46.

Carrasco-Núñez, G., Gomez-Tuena, A., and Rose, W.I., 1997, Volcanogenic sedimentation around Citlaltepetl (Pico de Orizaba) volcano and surroundings: Puerto Vallarta, Mexico, International Association of Volcanology and Chemistry of the Earth's Interior General Assembly, Excursion Guide, 32 p.

Cattermole, P., 1982, Meru: A Rift Valley giant: Volcano News, no. 11, p. 1–3.

Clague, D.A., and Denlinger, R.P., 1994, The role of olivine cumulates in destabilizing the flanks of Hawaiian volcanoes: Bulletin of Volcanology, v. 56, p. 425–434.

Clement, B.M., Conner, C.B., and Graper, G., 1993, Paleomagnetic estimate of the emplacement temperature of the long-runout Nevado de Colima volcanic debris avalanche deposit, Mexico: Earth and Planetary Science Letters, v. 120, p. 499–510.

Conway, F.M., Vallance. J.W., Rose, W.I., Johns, G.W., and Paniagua, S., 1992, Cerro Quemado, Guatemala: The volcanic history and hazards of an exogenous volcanic dome complex: Journal of Volcanology and Geothermal Research, v. 52, p. 303–323.

Crandell, D.R., 1989, Gigantic debris avalanche of Pleistocene age from ancestral Mount Shasta volcano, California, and debris-avalanche hazard zonation: U.S. Geological Survey Bulletin 1861, 32 p.

Crandell, D.R., Miller, C.D., Glicken, H.X., Christiansen, R.L., and Newhall, C.G., 1984, Catastrophic debris avalanche from ancestral Mount Shasta volcano, California: Geology, v. 12, p. 143–146.

Cruden, D.M., 1976, Major rock slides in the Canadian Rockies: Canadian Geotechnology Journal, v. 13, p. 8–20.

Davidson, G., 1884, Notes on the volcanic eruption of Mount St. Augustine, Alaska, October 6, 1883: Science, v. 3, p. 186–189.

Davies, T.R.H., 1982, Spreading of rock avalanche debris by mechanical fluidization: Rock Mechanics, v. 15, p. 9–24.

Day, S.J., 1996, Hydrothermal pore fluid pressure and the stability of porous, permeable volcanoes, *in* McGuire, W.J., Jones, A.P., and Neuberg, J., eds., Volcano instability on the earth and other planets: Geological Society [London] Special Publication 110, p. 77–93.

de Silva, S.L., Davidson, J.P., Croudace, I.W., and Escobar, A., 1993, Volcanological and petrological evolution of Volcan Tata Sabaya, SW Bolivia: Journal of Volcanology and Geothermal Research, v. 55, p. 305–335.

Denlinger, R.P., and Okubo, P., 1995, Structure of the mobile south flank of Kilauea volcano, Hawaii: Journal of Geophysical Research, v. 100, p. 24499–24507.

Downie, C., and Wilkinson, P., 1972, The geology of Kilimanjaro: Sheffield, England, University of Sheffield, Department of Geology, 253 p.

Dvorak, J.J., 1994, An earthquake cycle along the south flank of Kilauea volcano, Hawaii: Journal of Geophysical Research, v. 99, p. 9533–9541.

Eisbacher, G.H., and Clague, J.J., 1984, Destructive mass movements in high mountains: Hazard and management: Geological Survey of Canada Paper 84-16, 230 p.

Ellsworth, D., and Voight, B., 1995, Dike intrusion as a trigger for large earthquakes and the failure of volcano flanks: Journal of Geophysical Research, v. 100, p. 6005–6024.

Eppler, D.B., Fink, J., and Fletcher, R., 1987, Rheologic properties and kinematics of emplacement of the Chaos Jumbles rockfall avalanche, Lassen Volcanic National Park, California: Journal of Geophysical Research, v. 92, p. 3623–3633.

Erismann, T.H., 1979, Mechanisms of large landslides: Rock Mechanics, v. 12, p. 15–46.

Fairchild, L.H., 1987, The importance of lahar initiation processes: Reviews in Engineering Geology, v. 7, p. 51–61.

Fisher, R.V., Glicken, H.X., and Hoblitt, R.P., 1987, May 18, 1980, Mount St. Helens deposits in South Coldwater Creek, Washington: Journal of Geophysical Research, v. 92, p. 10267–10283.

Francis, P.W., and Self, S., 1987, Collapsing volcanoes: Scientific American, v. 256, no. 6, p. 90–97.

Francis, P.W., and Wells, G.L., 1988, Landsat Thematic Mapper observations of debris avalanche deposits in the Central Andes: Bulletin of Volcanology, v. 50, p. 258–278.

Francis, P.W., Gardeweg, M., Ramirez, C.F., and Rothery, D.A., 1985, Catastrophic debris avalanche deposit of Socompa volcano, northern Chile: Geology, v. 13, p. 600–603.

Frank, D., 1995, Surficial extent and conceptual model of hydrothermal system at Mount Rainier, Washington: Journal of Volcanology and Geothermal Research, v. 65, p. 51–80.

Geographical Survey Institute, 1982, Coastal area basic survey report, Shimabara area: Geographic Survey Institute (Japan) Technical Report D-3, no. 38, 195 p. text plus map, scale 1:25 000, 1 sheet.

Geronimo-Catane, S.G., 1997, Debris avalanche in the Philippines: Their occurrence, hazards, and mitigation measures: Puerto Vallarta, Mexico, International Association of Volcanology and Chemistry of the Earth's Interior General Assembly, Abstracts, p. 37.

Glicken, H., 1986, Rockslide: Debris avalanche of May 18, 1980, Mount St. Helens Volcano [Ph.D. thesis]: Santa Barbara, University of California, 303 p.

Glicken, H., 1991, Sedimentary architecture of large volcanic-debris avalanches, *in* Fisher, R.V., and Smith, G.A., eds., Sedimentation in volcanic settings: SEPM (Society for Sedimentary Geology) Special Publication 45, p. 99–106.

Glicken, H., 1996, Rockslide: Debris avalanche of May 18, 1980, Mount St. Helens volcano, Washington: U.S. Geological Survey Open-File Report 96-677, 90 p. Currently available in electronic version only at the Cascades Volcano Observatory web site: http://vulcan.wr.usgs.gov/Projects/Glicken/framework.html

Glicken, H., and Nakamura, Y., 1988, Restudy of the 1888 eruption of Bandai volcano, Japan, *in* Proceedings of the Kagoshima International Conference on Volcanoes: Tokyo, National Institute for Research Advancement, p. 392–395.

Glicken, H., Asmoro, P., Lubis, H., Frank, D., and Casadevall, T., 1987, The 1772 debris avalanche and eruption of Papandayan volcano, Indonesia, and hazards from future similar events [abs.]: Hilo, Hawaiian Symposium on How Volcanoes Work, p. 91.

Gorshkov, G.S., 1959, Gigantic eruption of the volcano Bezymianny: Bulletin of Volcanology, v. 21, p. 77–109.

Habib, P., 1975, Production of gaseous pore pressures during rockslides: Rock Mechanics, v. 7, p. 193–197.

Hayashi, J.N., and Self, S., 1992, A comparison of pyroclastic flow and debris avalanche mobility: Journal of Geophysical Research, v. 97, p. 9063–9071.

Hoblitt, R.P., Miller, C.D., and Vallance, J.W., 1981, Origin and stratigraphy of the deposit produced by the May 18 directed blast, *in* Lipman, P.W., and Mullineaux, D.R., eds., The 1980 eruptions of Mount St. Helens, Washington: U.S. Geological Survey Professional Paper 1250, p. 401–420.

Holcomb, R.T., and Searle, R.C., 1991, Large landslides from oceanic volcanoes: Marine Geotechnology, v. 10, p. 19–32.

Hsü, K., 1975, Catastrophic debris streams (sturzstroms) generated by rockfalls: Geological Society of America Bulletin, v. 86, p. 129–140.

Inman, D.L., 1952, Measures describing the size distribution of sediments: Journal of Sedimentary Petrology, v. 22, p. 125–145.

Inokuchi, T., 1988, Gigantic landslides and debris avalanches on volcanoes in Japan: Case studies on Bandai, Chokai, and Iwate Volcanoes (in Japanese

with English abstract): Report of the Natural Resources Center for Disaster Prevention, v. 41, p. 163–275.

Iverson, R.M., 1995, Can magma-injection and groundwater forces cause massive landslides on Hawaiian volcanoes?, *in* Ida, Y., and Voight, B., eds., Models of magmatic processes and volcanic eruptions: Journal of Volcanology and Geothermal Research, v. 66, p. 295–308.

Katayama, N., 1974, Old records of natural phenomena concerning the "Shimabara Catastrophe" (in Japanese with English abstract): Science Reports of the Shimabara Volcano Observatory, Kyushu University, Faculty of Science, v. 9, p. 1–45.

Kawachi, S., and Hayatsu, K., 1994, Debris avalanche and lahar deposits in the Yatsugatake volcanic chain and Myoko volcano group, central Japan: Journal of Natural Disaster Science, v. 16, p. 55–69.

Kent, P.E., 1966, The transport mechanism in catastrophic rock falls: Journal of Geology, v. 74, p. 79–83.

Kienle, J., Kowalik, Z., and Murty, T.S., 1987, Tsunamis generated by eruptions from Mount St. Augustine volcano, Alaska: Science, v. 236, p. 1442–1447.

Komorowski, J.-C., Glicken, H.X., and Sheridan, M.F., 1991, Secondary electron imagery of microcracks and hackly fracture surfaces in sand-size clasts from the 1980 Mount St. Helens debris-avalanche deposit: Implications for particle-particle interactions: Geology, v. 19, p. 261–264.

Komorowski, J.-C., Navarro, C., Cortés, R., Saucedo, R., Gavilanes, J.C., Siebe, C., Espíndola, J.-M., and Rodríguez, S., 1997, The Colima volcanic complex. 1. Quaternary multiple debris-avalanche deposits; 2. Historical pyroclastic sequences (1913, 1991, 1994): Puerto Vallarta, Mexico, International Association of Volcanology and Chemistry of the Earth's Interior General Assembly, Excursion Guide, 68 p.

Kowalik, Z., and Murty, T.S., 1992, Relevance of bathymetry for tsunami runup modeling: Marine Geodesy, v. 14, p. 273–283.

Leonov V.L., 1995, Lineaments, tectonic fractures, and mechanical behavior of Klyuchevskoi volcano: Volcanology and Seismology, v. 16, p. 627–648.

López, D.L., and Williams, S.N., 1993, Catastrophic volcanic collapse: Relation to hydrothermal processes: Science, v. 260, p. 1794–1796.

Luchhitta, B.K., 1979, Landslide in Valles Marineris, Mars: Journal of Geophysical Research, v. 84, p. 8097–8113.

Macias, J.L., García, A., Arce, J.L., Espíndola, J.M., Kormorowski, J.-C., and Scott, K., 1997, Late Pleistocene-Holocene cataclysmic eruptions at Nevado de Toluca and Jocotitlán volcanoes, central Mexico: Puerto Vallarta, Mexico, International Association of Volcanology and Chemistry of the Earth's Interior General Assembly, Excursion Guide, 63 p.

MacPhail, D.R., 1973, The geomorphology of the Río Teno lahar, central Chile: Geographical Review, v. 63, p. 517–532.

Major, J.J., and Voight, B., 1986, Sedimentology and clast orientations of the 18 May 1980 southwest-flank lahars, Mount St. Helens, Washington: Journal of Sedimentary Petrology, v. 56, p. 691–705.

Mason, A.C., and Foster, H.L., 1956, Extruded mudflow hills of Nirasaki, Japan: Journal of Geology, v. 64, p. 74–83.

Mathews, W.H., and McTaggart, K.C., 1969, The Hope landslide, British Columbia: Geological Association of Canada, Proceedings, v. 20, p. 65–75.

McEwen, A.S., and Malin, M.C., 1989, Dynamics of Mount St. Helens 1980 pyroclastic flows, rockslide-avalanche, lahars and blast: Journal of Volcanology and Geothermal Research, v. 37, p. 205–231.

McGuire, W.J., 1996, Volcano instability: A review of contemporary themes, *in* McGuire, W.J., Jones, A.P., and Neuberg, J., eds., Volcano instability on the earth and other planets: Geological Society [London] Special Publication 110, p. 1–23.

Melekestsev, I.V., Braitseva, O.A., Ponomareva, V.V., and Sulerzhitsky, L.D., 1990, Ages and dynamics of development of the active volcanoes of the Kurile-Kamchatka region: International Geology Review, v. 32, p. 436–448.

Melekestsev, I.V., Litasova S.N., and Sulerzhitskiy, L.D., 1992, The age and scale of catastrophic eruptions of the directed explosion type in the Avacha volcano (Kamchtaka) in the late Pleistocene: Volcanology and Seismology, v. 13, p. 135–146.

Melosh, H.J., 1979, Acoustic fluidization: A new geologic process?: Journal of Geophysical Research, v. 84, p. 7513–7520.

Mimura, K., Kawachi, S., Fujimoto, U., Taneichi, M., Hyuga, T., Ichikawa, S., and Koizumi, M., 1982, Debris avalanche hills and their natural remnant magnetization (in Japanese with English abstract): Nirasaki debris avalanche, central Japan: Journal of the Geological Society of Japan, v. 88, p. 653–663.

Moore, J.G., and Sisson, T.W., 1981, Deposits and effects of the May 18 pyroclastic surge, *in* Lipman, P.W., and Mullineaux, D.R., eds., The 1980 eruptions of Mount St. Helens, Washington: U.S. Geological Survey Professional Paper 1250, p. 421–438.

Moore, J.G., Clague, D.A., Holcomb, R.T., Lipman, P.W., Normark, W.R., and Torresan, M.E., 1989, Prodigious submarine landslides on the Hawaiian Ridge: Journal of Geophysical Research, v. 94, p. 17465–17484.

Moore, J.G., Normark, W.R., and Holcomb, R.T., 1994, Giant Hawaiian landslides: Annual Review of Earth and Planetary Sciences, v. 22, p. 119–144.

Moreno, R., 1991, The southern Andes volcanoes (33°–41°30′S), Chile: 6th Congreso Geológico Chileno—Guía de Excursión, PC-3, 26 p.

Murai, I., 1961, A study of the textural characteristics of pyroclastic flow deposits in Japan: Tokyo, Tokyo University, Bulletin of the Earthquake Research Institute, v. 39, p. 133–248.

Nakamura, Y., 1978, Geology and petrology of Bandai and Nekoma volcanoes: Tohoku University Science Reports, ser. 3, v. 14, p. 67–119.

Naranjo, J.A., Scott, K.M., and Hildreth, W.E., 1997, Highly mobile catastrophic debris avalanche of Planchon-Peteroa volcanic complex, southern Andes, Chile: Puerto Vallarta, Mexico, International Association of Volcanology and Chemistry of the Earth's Interior General Assembly, Abstracts, p. 107.

Neumann van Padang, M., 1939, Über die vielen tausend Hügel in westlichen Vorlande des Raoeng-Vulkans (Ostjava): De ingenieur in Nederlandsch-Indié, v. 6, no. 4, p. 35–41.

Noguchi, Y., and Ono, K., 1986, Historical-geographical study of natural hazards in Kyushu during the Tokugawa Era (in Japanese): Kyushu University College of General Education and Natural History, Social Geography Research Group Research Report Grant no. 59580150, 50 p.

Ogawa, T., and Homma, F., 1926, The geology of the Unzen volcanoes: Pan-Pacific Science Congress, Guidebook for Excursion E-1, 3, 4, 30 p.

Ota, K., 1969, Study on the collapses in the Mayu-yama (in Japanese with English abstract): Science Reports of the Shimabara Volcano Observatory, Kyushu University, Faculty of Science, v. 5, p. 6–35.

Ota, K., 1973, A study of hot springs on the Shimabara Peninsula (in Japanese with English abstract): Science Reports of the Shimabara Volcano Observatory, Kyushu University, Faculty of Science, v. 8, p. 1–33.

Palmer, B.A., Alloway, B.V., and Neall, V.E., 1991, Volcanic-debris-avalanche deposits in New Zealand: Lithofacies organization in unconfined, wet-avalanche flows, *in* Fisher, R.V., and Smith, G.A., eds., Sedimentation in volcanic settings: SEPM (Society for Sedimentary Geology) Special Publication 45, p. 89–98.

Pierson, T.C., 1985, Initiation and flow behavior of the 1980 Pine Creek and Muddy River lahars, Mount St. Helens, Washington: Geological Society of America Bulletin, v. 96, p. 1056–1069.

Pierson, T.C., and Costa, J.E., 1987, A rheologic classification of subaerial sediment-water flows, *in* Costa, J.E., and Wieczorek, G.F., eds., Debris flows/avalanches: Process, recognition, and mitigation: Reviews in Engineering Geology, v. VII, p. 1–12.

Reid, M.E., 1994, Transient thermal pressurization in hydrothermal systems: A cause of large-scale edifice collapse at volcanoes: Geological Society of America Abstracts with Programs, v. 26, p. 376.

Richter, D.H., Smith, R.L., Yehle, L.A., and Miller, T.P., 1979, Geologic map of the Gulkana A-2 quadrangle, Alaska: U.S. Geological Survey Geologic Quadrangle Map GQ-1260, scale 1:63 360, 1 sheet.

Robin, C., and Boudal, C., 1987, A gigantic Bezymianny-type event at the beginning of modern Popocatépetl: Journal of Volcanology and Geothermal Research, v. 31, p. 115–130.

Scheidegger, A.E., 1973, On the prediction of the reach of velocity of catastrophic landslides: Rock Mechanics, v. 5, p. 231–236.

Schuster, R.L., and Crandell, D.R., 1984, Catastrophic debris avalanches from volcanoes, *in* Proceedings of the 4th International Symposium on Landslides, Volume 1: Toronto, p. 567–572.

Scott, K.M., 1989, Magnitude and frequency of lahars and lahar-runout flows in the Toutle-Cowlitz River system: U.S. Geological Survey Professional Paper 1447-A, p. 1–74.

Scott, K.M., and Vallance, J.W., 1995, Debris flow, debris avalanche, and flood hazards at and downstream from Mount Rainier, Washington: U.S. Geological Survey Hydrologic Investigation Atlas HA-729, scale 1:100 000, 1 sheet, plus 9 p. text.

Scott, K.M., Pringle, P.T., and Vallance, J.W., 1995, Sedimentology, behavior, and hazards of debris flows at Mount Rainier, Washington: U.S. Geological Survey Professional Paper 1547, 56 p.

Sekiya, S., and Kikuchi, Y., 1889, The eruption of Bandai-san: Tokyo Imperial University College of Sciences Journal, v. 3, no. 2, p. 91–172.

Shreve, R.L., 1968, The Blackhawk landslide: Geological Society of America Special Paper, v. 108, 47 p.

Siebe, C., Komorowski, J.-C., and Sheridan, M.F., 1992, Morphology and emplacement of an unusual debris-avalanche deposit at Jocotitlán volcano, central Mexico: Bulletin of Volcanology, v. 54, p. 573–589.

Siebe, C., Abrams, M., and Sheridan, M.F., 1993, Two different types of debris avalanche deposits at Las Derrumbadas rhyolite domes, east-central Mexico, *in* Proceedings, International Association of Volcanology and Chemistry of the Earth's Interior Canberra Meeting: Canberra, Abstracts, p. 100.

Siebe, C., Abrams, M., and Macías, J.L., 1995, Derrumbes gigantes, depositos de avalancha de escombros y edad del actual cono del volcan Popocatépetl, *in* Volcan Popocatépetl estudios realizados durante la crisis de 1994–1995: Centro Nacional de Prevención de Desastres, Universidad Nacional Autónoma de México, Mexico D.F., p.195–220.

Siebert, L., 1984, Large volcanic debris avalanches: Characteristics of source areas, deposits, and associated eruptions: Journal of Volcanology and Geothermal Research, v. 22, p. 163–197.

Siebert, L., 1996, Hazards of large volcanic debris avalanches and associated eruptive phenomena, *in* Scarpa, R., and Tilling, R.I., eds., Monitoring and mitigation of volcano hazards: Berlin, Springer-Verlag, p. 541–572.

Siebert, L., Glicken, H., and Ui, T., 1987, Volcanic hazards from Bezymianny- and Bandai-type eruptions: Bulletin of Volcanology, v. 49, p. 435–459.

Siebert, L., Glicken, H., and Kienle, J., 1989, Debris avalanches and lateral blasts at Mount St. Augustine volcano, Alaska: National Geographic Research, v. 5, p. 232–249.

Siebert, L., Vallance, J.W., and Rose, W.I., 1994, Quaternary edifice failures at volcanoes in the Guatemalan highlands [abs.]: Eos (Transactions, American Geophysical Union), v. 75, p. 367.

Siebert, L., Begét, J.E., and Glicken, H., 1995, The 1883 and late prehistoric eruptions of Augustine volcano, Alaska, *in* Ida, Y., and Voight, B., eds., Models of magmatic processes and volcanic eruptions: Journal of Volcanology and Geothermal Research, v. 66, p. 367–395.

Siebert, L., Bronto, S., Supriatman, I., and Mulyana, R., 1996, Massive debris-avalanche deposit from Raung volcano, eastern Java, Indonesia [abs.]: Eos (Transactions, American Geophysical Union), v. 77, p. S291.

Simkin, T., and Siebert, L., 1994, Volcanoes of the world (second edition): Tucson, Arizona, Geoscience Press, 349 p.

Smith, G.A., and Lowe, D.R., 1991, Lahars: Volcano-hydrologic events and deposition in the debris flow–hyperconcentrated flow continuum, *in* Fisher, R.V., and Smith, G.A., eds., Sedimentation in volcanic settings: SEPM (Society for Sedimentary Geology) Special Publication 45, p. 59–70.

Smith, M.S., and Shepherd, J.B., 1996, Tsunami waves generated by volcanic landslides: An assessment of the hazard associated with Kick 'em Jenny, *in* McGuire, W.J., Jones, A.P., and Neuberg, J., eds., Volcano instability on the earth and other planets: Geological Society [London] Special Publication 110, p. 115–123.

Sousa, J., and Voight, B., 1991, Continuum simulation of flow failures: Geotechnique, v. 41, p. 515–538.

Sousa, J., and Voight, B., 1995, Multiple-pulsed debris avalanche emplacement at Mount St. Helens in 1980: Evidence from numerical continuum flow simulations, *in* Ida, Y., Glicken, H., and Voight, B., eds., Models of magmatic processes and volcanic eruptions: Journal of Volcanology and Geothermal Research, v. 66, p. 227–250.

Stoopes, G.R., and Sheridan, M.F., 1992, Giant debris avalanches from the Colima Volcanic Complex, Mexico: Implications for long-runout landslides (>100 km) and hazard assessment: Geology, v. 20, p. 299–302.

Takarada, S., 1991, Flow and depositional mechanisms of debris avalanche: A case study of Iwasegawa debris avalanche deposit, Tashirodake volcano, northern Japan (in Japanese with English absstract): Bulletin of the Volcanological Society of Japan, v. 36, p. 11–23.

Ui, T., 1983, Volcanic dry avalanche deposits: Identification and comparison with nonvolcanic debris stream deposits, *in* Aramaki, S., and Kushiro, I., eds,. Arc volcanism: Journal of Volcanology and Geothermal Research, v. 18, p. 135–150.

Ui, T., 1987, Discrimination between debris avalanches and other volcaniclastic deposits, *in* Latter, J.H., ed., Volcanic hazards: Berlin, Springer-Verlag, p. 201–209.

Ui, T., and Glicken, H., 1986, Internal structural variations in a debris-avalanche deposit from ancestral Mount Shasta, California, USA: Journal of Volcanology and Geothermal Research, v. 48, p. 189–194.

Ui, T., Kawachi, S., and Neall, V.E., 1986a, Fragmentation of debris avalanche material during flowage: Evidence from the Pungarehu Formation, Mount Egmont, New Zealand: Journal of Volcanology and Geothermal Research, v. 27, p. 255–264.

Ui, T., Yamamoto, H., and Suzuki, K., 1986b, Characterization of debris avalanche deposits in Japan, *in* Kushiro, I., ed., M. Sakuyama and H. Fukuyama Memorial Volume: Journal of Volcanology and Geothermal Research, v. 29, p. 231–243.

Ui, T., and Fujiwara, H., 1993, Debris-avalanche database, *in* Aramaki, S., ed., Scale and characteristics of volcanic disasters, prediction of natural disasters and prevention measures for society (in Japanese): Natural Disaster Science Coordination Research Group, Ministry of Education Science Research Fund (Mombusho) Priority Area Research Report, no. A-4-5, p. 177–188.

Vallance, J.W., Siebert, L., Rose, W.I., Jr., Girón, J.R., and Banks, N.G., 1995, Edifice collapse and related hazards in Guatemala, *in* Ida, Y., and Voight, B., eds., Models of magmatic processes and volcanic eruptions: Journal of Volcanology and Geothermal Research., v. 66, p. 337–355.

van Wyk de Vries, B., and Borgia, A., 1996, The role of basement in volcano deformation, *in* McGuire, W.J., Jones, A.P., and Neuberg, J., eds., Volcano instability on the earth and other planets: Geological Society [London] Special Publication 110, p. 95–110.

Voight, B., Glicken, H., Janda, R.J., and Douglass, P.M., 1981, Catastrophic rockslide avalanche of May 18, *in* Lipman, P.W., and Mullineaux, D.R., eds., The 1980 eruptions of Mount St. Helens, Washington: U.S. Geological Survey Professional Paper 1250, p. 347–378.

Voight, B., Janda, R.J., Glicken, H., and Douglass, P.M., 1983, Nature and mechanics of the Mount St. Helens rockslide-avalanche of 18 May 1980: Geotechnique, v. 33, p. 243–273.

Voight, B., Janda, R.J., Glicken, H., and Douglass, P.M., 1985, Reply to discussion: Nature and mechanics of the Mount St. Helens rockslide-avalanche of 18 May 1980: Geotechnique, v. 35, p. 357–368.

Voight, B., Belousova, M.G., and Belousov, A.B., 1994, Magmatic-groundwater interactions with edifice collapse and explosive volcanism: Example from repetitive events at Shiveluch volcano, Kamchatka: Geological Society of America Abstracts with Programs, v. 26, p. 376.

Wadge, G., Francis, P.W., and Ramirez, C.F., 1995, The Socompa collapse and avalanche event, *in* Ida, Y., and Voight, B., eds., Models of magmatic processes and volcanic eruptions: Journal of Volcanology and Geothermal Research, v. 66, p. 309–336

Waitt, R.B., Jr., 1981, Devastating pyroclastic density flow and attendant air fall of May 18: Stratigraphy and sedimentology of deposits, *in* Lipman, P.W., and Mullineaux, D.R., eds., The 1980 eruptions of Mount St. Helens, Washington: U.S. Geological Survey Professional Paper 1250, p. 439–460.

Waitt, R.B., and Begét, J.E., 1996, Provisional geologic map of Augustine volcano, Alaska: U.S. Geological Survey Open-File Report 96–516, 44 p.

Walker, G.P.L., 1971, Grain-size characteristics of pyroclastic deposits: Journal of Geology, v. 79, p. 696–714.

Wilson, C.J.N., 1980, The role of fluidization with emplacement of pyroclastic flows: An experimental approach: Journal of Volcanology and Geothermal Research, v. 8, p. 231–249.

Yarnold, J.C., and Lombard, J.P., 1989, A facies model for large rock-avalanche deposits formed in dry climates, *in* Colburn, I.P., Abbott, P.L., and Minch, J. eds., Conglomerates in basin analysis: A Symposium Dedicated to A.O. Woodford: Pacific Section, SEPM (Society for Sedimentary Geology), v. 62, p. 9–31.

Yehle, L.A., Nichols, D.R., 1980, Reconnaissance map and description of the Chetaslina volcanic debris flow (new name), southeastern Copper River basin and adjacent areas, south-central Alaska: U.S. Geological Survey Miscellaneous Field Studies Map MF-1209, scale 1:250000, 1 sheet.

Yonechi, Y., 1987, A new hypothesis on the collapse of Bandai-san volcano in 1888: Science Reports of Tohoku University, ser. 7, v. 37, p. 159–173.

Yoshimoto, M., and Ui, T., 1997, 1640 eruption of Hokkaido Komagatake volcano, Japan: Puerto Vallarta, Mexico, International Association of Volcanology and Chemistry of the Earth's Interior General Assembly, Abstracts, p. 133.

MANUSCRIPT SUBMITTED MARCH 12, 1996;
ACCEPTED BY THE SOCIETY NOVEMBER 30, 2001.

Printed in the USA